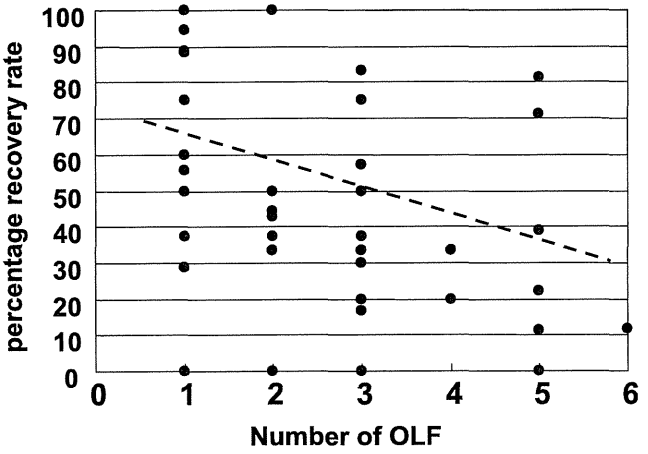

Fig. 2. Relationship between percentage recovery rate and the number of levels affected by OLF; r=−0.34; 95% confidence interval, −12.43< r<−0.64; p=.031. OLF, ossification of the ligamentum flavum.

The highest values of percentage recovery rates in our study and in the two previous ones [12,13] were lower than the highest values of percentage recovery rates, 55 (60%) of 92 patients and 24 (50%) of 49 patients, respectively, in our two reports [35,37] of surgery for cervical OPLL.

Speculatively, poor postsurgical recovery might be a consequence of the vulnerability of the thoracic spinal cord to poor blood supply. In our series, all patients had posterior decompression without spinal fusion. Because OLF affects the posterior part of the spinal cord, posterior decompression such as laminectomy is reasonable.

Numerous reports [7,9,12,38] noted that OLF frequently develops in the lower thoracic spine in middle-age men. However, thoracic OLF frequently has concurrent cervical or lumbar lesions, or both [7,8,10,12,13,38]. Park et al. [20] introduced a term, "tandem ossification," for patients with thoracic OLF associated with cervical OPLL. Furthermore, a lesion near the conus medullaris may result in complex neurologic findings [39]. In our study, concurrent lesions were thoracic OPLL, thoracic disc herniation, lumbar spinal stenosis, cervical OPLL, and lumbar disc herniation. Ten (24%) patients underwent surgery for concurrent cervical or lumbar lesions. Coexisting spinal lesions may complicate symptoms of and physical findings in OLF. Therefore, a precise neurologic examination should be carried out before deciding on how to treat patients with thoracic OLF.

Table 6
Intramedullary change and surgical outcome

Variables	Intramedullary change on MRI		p Value
	No	Yes	
Male; female	5; 4	9; 3	.397
Age (y) at surgery (mean [SD])	66.1 (8.9)	56.5 (12.8)	.069
JOA score (mean [SD])			
Presurg	4.7 (2.2)	4.3 (1.7)	.613
1-Mo postsurg	6.7 (1.9)	5.8 (1.5)	.246
Final follow-up	7.9 (2.1)	6.5 (1.7)	.107
% Recovery rate			
1-Mo postsurg	31.6 (18.5)	22.2 (14.2)	.204
Final follow-up	54.9 (28.6)	32.2 (22.9)	.057

MRI, magnetic resonance imaging; SD, standard deviation; JOA, Japanese Orthopaedic Association score; presurg, presurgical; postsurg, postsurgical.

Use of spinal fusion to treat TM caused by OLF is controversial. Kyphotic spinal deformity after thoracic laminectomy may cause neurologic deterioration or localized back pain in the cervical and lumbar spine during long-term follow-up. However, in retrospectively evaluating surgery for thoracic OLF in a large case series (58 patients), Aizawa et al. [40] reported an increase in kyphosis of fewer than 2° occurred in more than half and that no additional surgeries were required for treating increased kyphotic deformity. Therefore, we believe that spinal fusion is not always necessary for treating thoracic OLF.

The two previous reports [12,13] about outcomes of decompression surgery for TM caused by OLF noted several factors affecting outcome. Years of symptoms presurgically is related to poor outcome [12,13]. Possibly, lengthy duration of spinal cord compression causes irreversible nerve tissue damage. In our study, however, the relationship between presurgical duration of symptoms and percentage recovery rate was not statistically significant. Some patients in our study might not have been able to accurately note the time of onset of symptoms.

Precise history taking is mandatory, but symptoms are subjective. We believed that objective findings, such as those from neurologic and radiologic examinations, were important to evaluate the factors affecting postsurgical recovery. Postsurgical neurologic condition depends on the presurgical severity of myelopathy [13]. In accordance with this finding, our results showed that the more severe the neurologic symptoms, the more severe was the postsurgical neurologic condition. Impairment of joint position sense in the big toe was the most important predictor of the highest postsurgical JOA score and the lowest percentage recovery rate in multiple linear regression analyses.

Joint position sense is one way to examine the deep senses, as are as deep touch, vibration, and two-point sensations [41]. In patients with cervical myelopathy, Takayama et al. [31] analyzed knee joint position sense, and Yoshikawa et al. [32] and Doita et al. [41] examined hand function and postural stability. They found that these proprioceptive senses are impaired in patients with cervical myelopathy. We are unaware of any reports about proprioceptive sense in patients with TM.

Deep sensations are carried in the dorsal column in the spinal cord. Inability to detect joint position sense in space reflects dysfunction of the dorsal column. Because OLF is in the posterior part of the spinal canal, it may easily cause dysfunction of the dorsal column. Consequently, examination of position sense in the big toe is an important predictor of postsurgical recovery. In addition, we found that

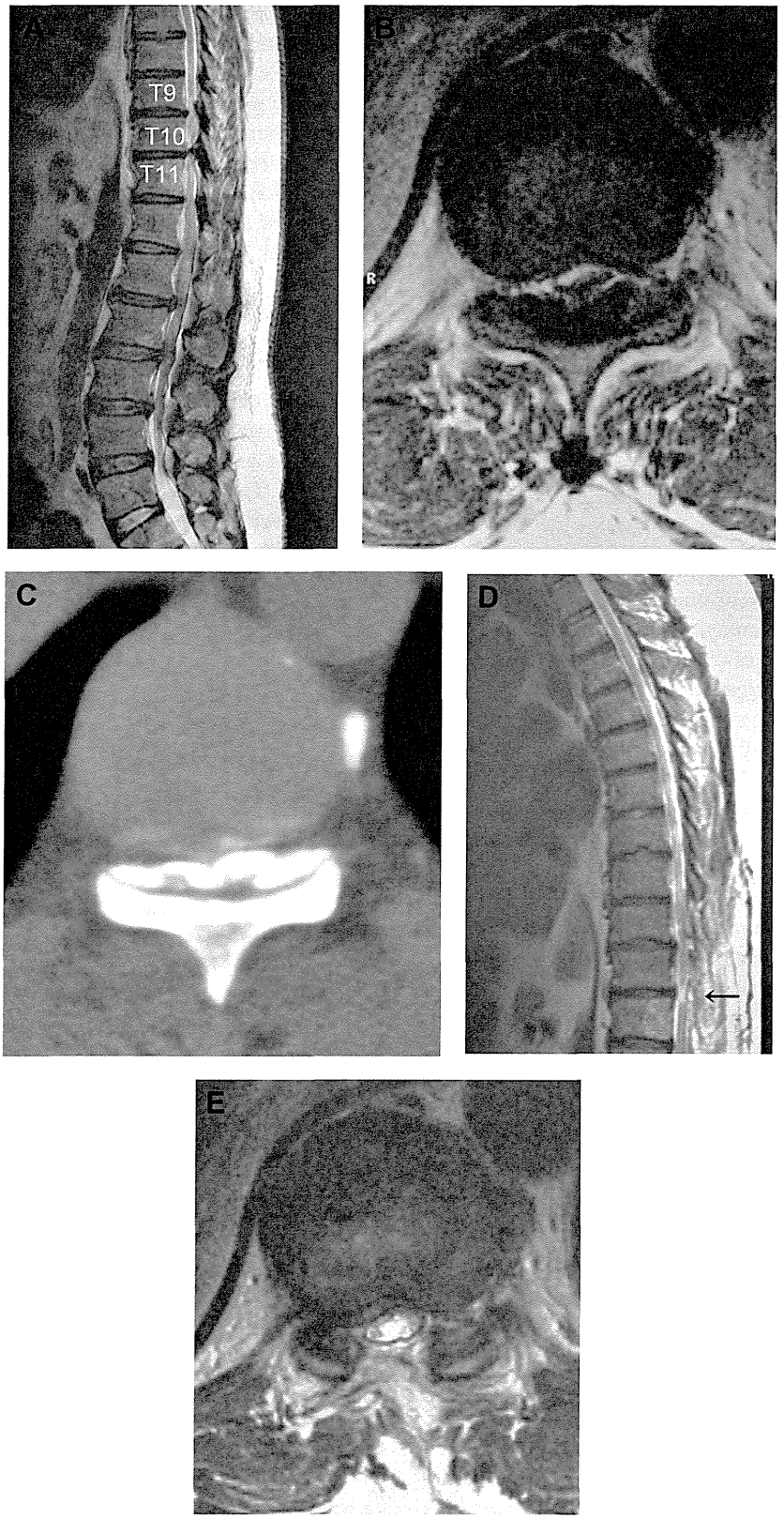

Fig. 3. Radiographic findings in Patient 21. (A) Presurgical sagittal T2-weighted magnetic resonance imaging (MRI) view showing spinal cord compression at T9–T10 and T10–T11 levels. (B) Presurgical axial T2-weighted MRI showing spinal cord compression at T10–T11 and intramedullary signal change. (C) Computed tomography myelogram at T10–T11 level. (D) Postsurgical sagittal T2-weighted MRI showing decompression of the spinal cord at T9–T10 and T10–T11 (arrow). (E) Postsurgical axial T2-weighted MRI view revealing decompression of the spinal cord at T10–T11, but remaining presence of intramedullary signal change.

patients with higher numbers of affected levels of OLF had poorer percentage postsurgical recovery. This finding might indicate that prolonged spinal cord compression caused by OLF results in severe neural damage in the thoracic spinal cord.

Only 21 of the 41 patients underwent presurgical MRI because this study included TM patients who had surgery before early 1990s. Interestingly, however, patients whose MRIs showed presurgical intramedullary signal change had poorer postsurgical recovery than patients whose MRIs did not show this change. The relationship between presurgical intramedullary signal intensity change and postsurgical recovery has been well studied in patients with cervical myelopathy. Yukawa et al. [42] prospectively evaluated intramedullary signal intensity change in 104 patients with cervical myelopathy. They concluded that the patients with the greatest signal change had the worst postsurgical recovery.

Intramedullary signal change in the spinal cord appears in the pathologic changes, such as loss of nerve cells, gliosis, edema in gray or white matter, Wallerian degeneration, and demyelination [43,44]. In our study, seven of the nine patients whose presurgical MRIs showed intramedullary signal change still had intramedullary signal change observed on postsurgical MRI. This result might indicate that the patients with postsurgical signal change had irreversible spinal cord changes resulting from compression caused by OLF. On the other hand, the two patients whose postsurgical MRI did not show signal change might have had a reversible spinal cord lesion.

The study had limitations. The sample size was small, making it possible that statistically significant differences were not detected. For example, postsurgical JOA scores and percentage recovery rates of scores in patients whose presurgical MRIs had shown intramedullary signal change were less than those whose presurgical MRIs had not shown signal change. We regarded this finding as clinically important. Another limitation was that postsurgical evaluations of PTR and ATR were not compared with presurgical PTR and ATR because postsurgical evaluations were not found in the medical records of most patients.

An excellent postoperative prognosis is not always possible in patients with TM caused by OLF. It may be important to check for impairment of joint position sense in the big toe, the number of levels affected by OLF, and presurgical intramedullary signal change on MRI before continuing to surgery.

Acknowledgments

The authors thank Hideki Origasa, PhD, for the statistical analysis. The authors contracted with Michael S. Altus, PhD, ELS, of Intensive Care Communications, Inc., Baltimore, MD, USA, to edit their initial manuscript. The authors thank Dr Origasa and Dr Altus for their excellent services. The authors maintained complete control over the direction and content of the manuscript.

References

[1] Tsukimoto H. On an autopsied case of compression myelopathy with a callus formation in the cervical spinal canal. [in Japanese]. Nihon Geka Hokan 1960;29:1003–7.
[2] Ono K, Yonenobu K, Miyamoto S, Okada K. Pathology of ossification of the posterior longitudinal ligament and ligamentum flavum. Clin Orthop Relat Res 1999;359:18–26.
[3] Yayama T, Uchida K, Kobayashi S, et al. Thoracic ossification of the human ligamentum flavum: histopathological and immunohistochemical findings around the ossified lesion. J Neurosurg Spine 2007;7:184–93.
[4] The Investigation Committee on OPLL of the Japanese Ministry of Public Health and Welfare. The ossification of the posterior longitudinal ligament of the spine (OPLL). J Jpn Orthop Assoc 1981;55:425–40.
[5] Miyasaka K, Kaneda K, Ito T, et al. Ossification of spinal ligaments causing thoracic radiculomyelopathy. Radiology 1982;143:463–8.
[6] Otani K, Aihara T, Tanaka A, Shibasaki K. Ossification of the ligamentum flavum of the thoracic spine in adult kyphosis. Int Orthop 1986;102:135–9.
[7] Aizawa T, Sato T, Sasaki H, et al. Thoracic myelopathy caused by ossification of the ligamentum flavum: clinical features and surgical results in the Japanese population. J Neurosurg Spine 2006;56:514–9.
[8] Yonenobu K, Ebara S, Fujiwara K, et al. Thoracic myelopathy secondary to ossification of the spinal ligament. J Neurosurg 1987;66:511–8.
[9] Okada K, Oka S, Tohge K, et al. Thoracic myelopathy caused by ossification of the ligamentum flavum. Clinicopathologic study and surgical treatment. Spine 1991;16:280–7.
[10] Hanakita J, Suwa H, Ohta F, et al. Neuroradiological examination of thoracic radiculomyelopathy due to ossification of the ligamentum flavum. Neuroradiology 1990;32:38–42.
[11] Nishiura I, Isozumi T, Nishihara K, et al. Surgical approach to ossification of the thoracic yellow ligament. Surg Neurol 1999;51: 368–72.
[12] Shiokawa K, Hanakita J, Suwa H, et al. Clinical analysis and prognostic study of ossified ligamentum flavum of the thoracic spine. J Neurosurg 2001;94:221–6.
[13] Miyakoshi N, Shimada Y, Suzuki T, et al. Factors related to long-term outcome after decompressive surgery for ossification of the ligamentum flavum of the thoracic spine. J Neurosurg 2003;99:251–6.
[14] Hirabayashi H, Ebara S, Takahashi J, et al. Surgery for thoracic myelopathy caused by ossification of the ligamentum flavum. Surg Neurol 2008;69:114–6.
[15] Li KK, Chung OM, Chang YP, So YC. Myelopathy caused by ossification of ligamentum flavum. Spine 2002;27:E308–12.
[16] Liao CC, Chen TY, Jung SM, Chen LR. Surgical experience with symptomatic thoracic ossification of the ligamentum flavum. J Neurosurg Spine 2005;2:34–9.
[17] Li F, Chen Q, Xu K. Surgical treatment of 40 patients with thoracic ossification of the ligamentum flavum. J Neurosurg Spine 2006;4:191–7.
[18] Kuh SU, Kim YS, Cho YE, et al. Contributing factors affecting the prognosis surgical outcome for thoracic OLF. Eur Spine J 2006;15: 485–91.
[19] Park BC, Min WK, Oh CW, et al. Surgical outcome of thoracic myelopathy secondary to ossification of ligamentum flavum. Joint Bone Spine 2007;74:600–5.
[20] Park JY, Chin DK, Kim KS, Cho YE. Thoracic ligament ossification in patients with cervical ossification of the posterior longitudinal ligaments: tandem ossification in the cervical and thoracic spine. Spine 2008;33:E407–10.
[21] Omojola MF, Cardoso ER, Fox AJ, et al. Thoracic myelopathy secondary to ossified ligamentum flavum. J Neurosurg 1982;56:448–50.

[22] Shiraishi T, Crock HV, Lewis P. Thoracic myelopathy due to isolated ossification of the ligamentum flavum. J Bone Joint Surg Br 1995;77: 131–3.
[23] van Oostenbrugge RJ, Herpers MJ, de Kruijk JR. Spinal cord compression caused by unusual location and extension of ossified ligamenta flava in a Caucasian male. A case report and literature review. Spine 1999;24:486–8.
[24] Epstein NE. Ossification of the yellow ligament and spondylosis and/or ossification of the posterior longitudinal ligament of the thoracic and lumbar spine. J Spinal Disord 1999;12:250–6.
[25] Tokala DP, Lam KS, Prince HG. Ossification of the proximal thoracic ligamenta flava causing acute myelopathy in a Caucasian: case report and literature review. Spinal Cord 2007;45:310–3.
[26] Xu R, Sciubba DM, Gokaslan ZL, Bydon A. Ossification of the ligamentum flavum in a Caucasian man. J Neurosurg Spine 2008;9:427–37.
[27] Ben Hamouda K, Jemel H, Haouet S, Khaldi M. Thoracic myelopathy caused by ossification of the ligamentum flavum: a report of 18 cases. J Neurosurg 2003;99:157–61.
[28] Smith DE, Godersky JC. Thoracic spondylosis: an unusual cause of myelopathy. Neurosurgery 1987;20:589–93.
[29] Ross RT. Dissociated loss of vibration, joint position and discriminatory tactile senses in disease of spinal cord and brain. Can J Neurol Sci 1991;18:312–20.
[30] MacFadyen DJ. Posterior column dysfunction in cervical spondylotic myelopathy. Can J Neurol Sci 1984;11:365–70.
[31] Takayama H, Muratsu H, Doita M, et al. Impaired proprioception in patients with cervical myelopathy. Spine 2004;30:83–6.
[32] Yoshikawa M, Doita M, Okamoto K, et al. Impaired postural stability in patients with cervical myelopathy. Evaluation by computerized static stabilometry. Spine 2008;33:E460–4.
[33] Nardone A, Galante M, Grasso M, Schieppati M. Stance ataxia and delayed leg muscle responses to postural perturbations in cervical spondylotic myelopathy. J Rehabil Med 2008;40:539–47.
[34] Zeidman SM, Ducker TB. Evaluation of patients with cervical spine lesion. In: Clark CR, ed. The cervical spine. 3rd ed. Philadelphia, PA: Lippincott-Raven Publishers 143-161, 1998.
[35] Kawaguchi Y, Kanamori M, Ishihara H, et al. Minimal 10-year follow up after en block cervical laminoplasty. Clin Orthop Relat Res 2003;411:129–39.
[36] Nurick S. The pathogenesis of the spinal cord disorder associated with cervical spondylosis. Brain 1972;95:87–100.
[37] Iwasaki M, Kawaguchi Y, Kimura T, Yonenobu K. Long-term results of expansive laminoplasty for ossification of the posterior longitudinal ligament of the cervical spine: more than 10 years follow up. J Neurosurg Spine 2002;96:180–9.
[38] Aizawa T, Sato T, Sasaki H, et al. Results of surgical treatment for thoracic myelopathy: minimum 2-year follow-up study in 132 patients. J Neurosurg Spine 2007;7:13–20.
[39] Harrop JS, Naroji S, Maltenfort MG, et al. Neurologic improvement after thoracic, thoracolumbar, and lumbar spinal cord (conus medullaris) injuries. Spine 2010;36:21–5.
[40] Aizawa T, Sato T, Ozawa H, et al. Sagittal alignment changes after thoracic laminectomy in adults. J Neurosurg Spine 2008;8:510–6.
[41] Doita M, Sakai H, Harada T, et al. The influence of proprioceptive impairment on hand function in patients with cervical myelopathy. Spine 2006;31:1580–4.
[42] Yukawa Y, Kato F, Yoshihara H, et al. MR T2 image classification in cervical compression myelopathy: predictor of surgical outcomes. Spine 2007;32:1675–8.
[43] Ito T, Oyanagi K, Takahashi H, et al. Cervical spondylotic myelopathy. Clinicopathologic study on the progression pattern and thin myelinated fibers of the lesions of seven patients examined during complete autopsy. Spine 1996;21:827–33.
[44] Takahashi M, Yamashita Y, Sakamoto Y, Kojima R. Chronic cervical cord compression: clinical significance of increased signal intensity on MR images. Radiology 1989;173:219–24.

Hindawi Publishing Corporation
Advances in Mechanical Engineering
Volume 2013, Article ID 928071, 7 pages
http://dx.doi.org/10.1155/2013/928071

Hindawi

Research Article

A Biomechanical Study on Laminectomy and Dekyphosis for Thoracic Ossification of the Posterior Longitudinal Ligament

Tadaki Okayama,[1] Hideki Murakami,[1] Satoru Demura,[1] Norio Kawahara,[2] Katsuro Tomita,[1] and Hiroyuki Tsuchiya[1]

[1] *Department of Orthopaedic Surgery, Kanazawa University, Kanazawa 920-8641, Japan*
[2] *Department of Orthopaedic Surgery, Kanazawa Medical University, Kanazawa 920-8641, Japan*

Correspondence should be addressed to Tadaki Okayama; tokayama@sky.plala.or.jp

Received 1 August 2013; Revised 7 September 2013; Accepted 9 September 2013

Academic Editor: Magd Abdel Wahab

We have successfully employed two-step circumspinal decompression for the treatment of thoracic OPLL. In the first step, laminectomy is performed according to the ossified lesion, and then correcting fixation of kyphosis (dekyphosis) is performed using instrumentation. In this study, we reconstructed the first step by a FEM. A commercially available FEM of the human body, THUMS, was used for the modeling of the operative procedure. The spinal cord and OPLL were incorporated into this model. After applying imposed displacement to OPLL, mechanical stress on the spinal cord was measured before or after posterior decompression at the occupying rates in the spinal canal between 0 and 70% in this model. When the occupancy rate was greater than 60%, the stress decreased after decompression compared to before decompression. The stress decreased by up to 52.3%. For reconstruction of dekyphosis, the change in the stress was analyzed after imposed displacement by which the spine was decreased: the cobb angle decreased by 10 degrees between T7 to T11. As a result, the stress further decreased by 14.6%. The present study proved the usefulness of posterior decompression and dekyphosis in order to reduce the pressure of the spinal cord in circumspinal decompression.

1. Introduction

Ossification of the posterior longitudinal ligament (OPLL) is an intractable disease characterized by spinal canal narrowing and spinal cord compression due to ossification/enlargement of the posterior longitudinal ligament extending craniocaudally along the posterior surfaces of the vertebral bodies, resulting in spinal paralysis.

We performed a 2-step surgery (posterior decompression and fusion as the first step and anterior decompression as the second step) for OPLL in the thoracic spine to achieve circumspinal decompression and obtained favorable results [1]. At the time of posterior decompression and fusion, correcting fixation of kyphosis (dekyphosis) in addition to laminectomy had been performed [2, 3]. Dekyphosis may lead to indirect spinal cord decompression, producing favorable results.

Therefore, we produced finite element models (FEMs) of OPLL in the thoracic spine, including the thoracic spinal cord, and mechanically evaluated the effects of posterior decompression and fusion, with dekyphosis as our routine method on the spinal cord, using computer simulation.

2. Methods

2.1. Posterior Decompression and Fusion with Dekyphosis. In posterior decompression and fusion as the routine method, laminectomy in the ligament ossification area is performed, followed by posterior decompression. Subsequently, left and right pedicle screws are inserted into the cranial and caudal sides of the ossification area, and rods with curvature about 15 degrees smaller than the kyphosis angle are placed into the screw heads for 5 to 10 degrees reduction in kyphosis and stabilization (Figure 1).

2.2. Production and Analysis of FEMs. To utilize the total human model for safety (THUMS: Toyota technical development) as a FEM of the human body in this study, the following

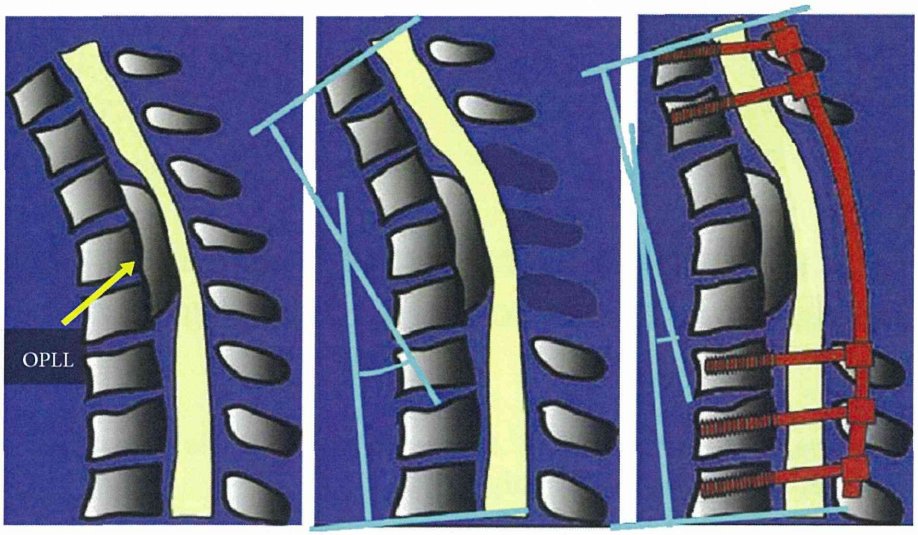

FIGURE 1

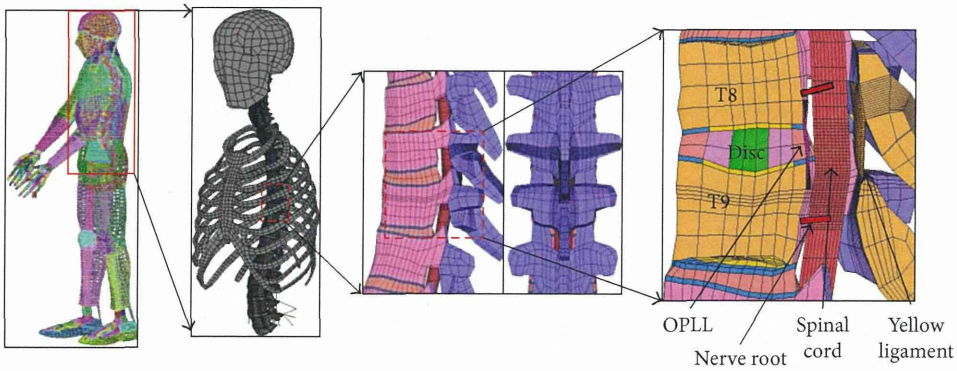

FIGURE 2

revisions were made. The THUMS is an FEM model of the whole human body for crash analysis (Figure 2(a)). The model used in this study was for an assumed female in the standing position (height, 150 cm; weight, 50 kg; and age, 40–50 years). From this THUMS, the head, spine, and ribs were extracted, and modifications were made to obtain a continuous model in this study (Figure 2(b)). The spinal cord, spinal nerve roots, and OPLL were added to the original model for this study (Figure 2(c)).

Since Tsuzuki [4] reported that the spinal canal area is smaller at the 8th thoracic spine (T8) and T9 than at other levels, OPLL between T8 and T9 may induce severe myelopathy. Therefore, the model was constructed assuming OPLL between T8 and T9. The shape of OPLL was assumed to be the simple segmental type. The ligamentum flavum was assumed to have a simple shape with a maximum thickness of 2 mm. The material constants of the ligament were inputted.

The spinal cord was added so that it could pass through the midline of the spinal canal. We performed modeling, assuming that the spinal cord extends to L5. Since ossification at T8-T9 was assumed in this study, the thickness of the spinal cord at T8-T9 was used. The thickness of the spinal cord at this level was determined based on the measurement results on MRI images of 20 healthy adults. As a result of the determination of the percentage of the anteroposterior diameter of the spinal cord to that of the spinal canal at T8-T9, the mean value was 50% (45%–60%). Therefore, the size of the spinal cord was determined to be 6.5 mm (50% of the anteroposterior diameter of the spinal canal at T8-T9). The transverse diameter was determined to be 10 mm as the general size [5]. There are no generally accepted opinions about Young's moduli of the gray and white matters of the spinal cord [6, 7]. Therefore, in this study, to simplify the model, we used the results of tensile tests performed by Bilston and Thibault [8] using the human cervical spinal cord without distinction between the gray and white matters. Spinal nerve roots from the 1st cervical spinal nerve to the 5th lumbar spinal nerve were constructed. Each nerve root

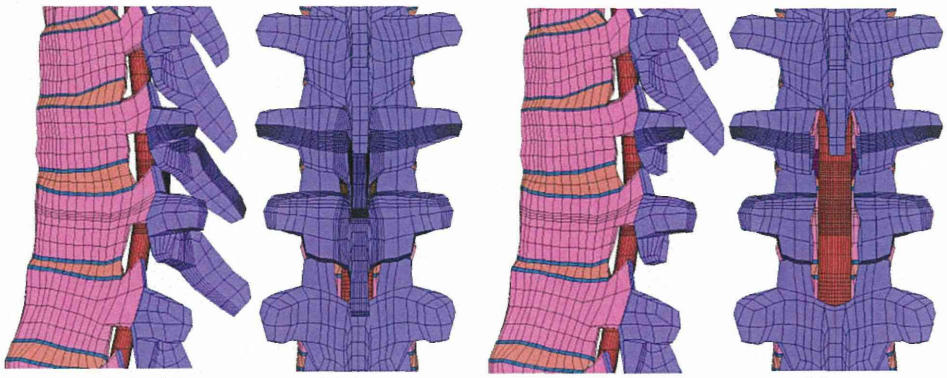

Predecompression model
(T7–T10)
(a)

Postdecompression model
(T7–T10)
(b)

FIGURE 3

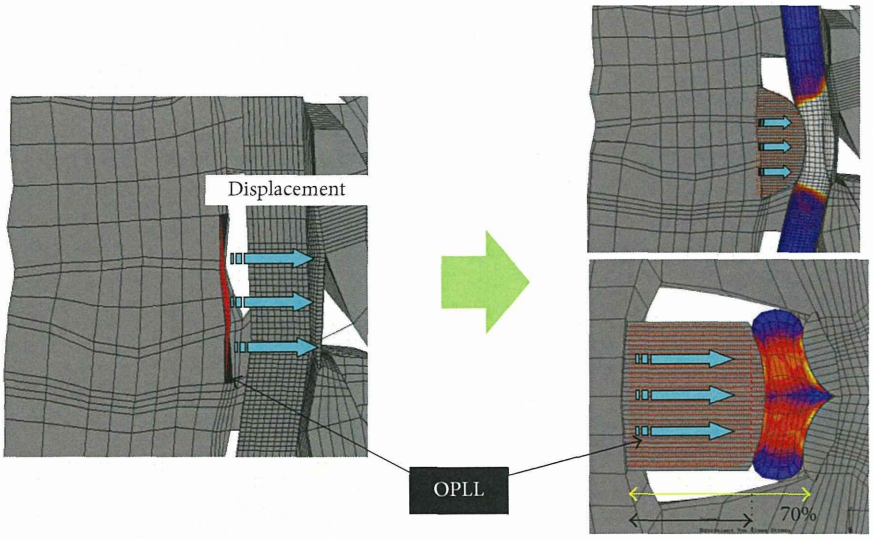

FIGURE 4

was established so that it would originate in the spinal cord at the middle level of each vertebral body and be fixed on the posterolateral side of the vertebral body corresponding to the intervertebral foramen. The material constants of the nerve root were determined based on the report by Scifert et al. [9].

In this study, to evaluate the mechanical effects of spinal cord decompression, two models (before and after posterior decompression) were produced. The model after posterior decompression was produced by removing the vertebral arches (the posterior part of a vertebra) of T8 and T9 from the preoperative model (Figure 3).

The material constants of this analytic model were the same as those used in the THUMS. The material constants of OPLL, which were newly added, were assumed to be similar to those of cortical bone in the thoracic spine (Table 1). Further, 248.7(N) corresponding to the weight of the upper half body was applied to the center of gravity of the trunk, and analysis was performed [10]. As having restraining conditions, the intervertebral disc and spinal cord on the lower surface of L5 were completely fixed.

There have been various studies on the relationship between the occupation rate and symptoms [11–13]. Matsunaga et al. [14] reported that myelopathy developed in all 45 patients with an occupation rate ≥60%. Therefore, in this study, to create an occupation rate ≥60%, analysis was performed by changing the size of OPLL so that the occupation rate became 70%, respectively. Changes in OPLL were reproduced by applying forced displacement to the surface (Figure 4).

Under these conditions, analysis and comparison were performed using the model before posterior decompression and model after laminectomy representing posterior decompression. In addition, mechanical evaluation after posterior decompression followed by thoracic dekyphosis was performed. Since the mean dekyphosis angle in the 15 patients that we surgically treated was 6 degrees (5–10 degrees), the maximum dekyphosis angle in this study was

Table 1: Material constants of the model.

Part of the model	Young's modulus [MPa]	Poisson's ratio
Cancellous bone		
C1–C7	70.00	0.300
T1–T12	203.0	0.450
L1–L5	70.00	0.450
Rib	40.00	0.450
Cortical bone		
C1–C7	5000	0.300
T1–T12 (front)	5000	0.300
T1–T12 (rear)	4000	0.300
L1–L5	1000	0.450
Rib	18900	0.300
Rib cartilage	24.50	0.400
Cartilage	12.60	0.400
Annulus in	0.200	0.400
Annulus out	13.30	0.400
Nucleus pulposus		
C1–C7	0.198	0.499
L1–L5	0.013	0.499
T1–T12	0.200	0.499
Vertebral endplate	500.0	0.400
Cartilaginous endplate	24.00	0.400
Brain	0.102	0.499
Lamina	8000	0.220
Diploe	200.0	0.220
Face	5540	0.220
OPLL, OLF	5000	0.300
Iliolumbar ligament	10.00	0.000
LCL, SCL	52.00	0.000
SSL, ISL, LF, ITL	10.00	0.300
ALL, PLL	20.00	0.400
ALL, PLL (cervical)	3.250	0.220
LN (C2–C7)	3.010	0.220
Nerve root	31.50	0.450

ALL: anterior longitudinal ligament; ISL: interspinous ligament; ITL: intertransverse ligament; LCL: lateral costotransverse ligament; LN: ligamentum nuchae; PLL: posterior longitudinal ligament; SCL: superior costotransverse ligament; SSL: supraspinous ligament.
Young's modulus is a measure of the stiffness of an isotropic elastic material in solid mechanics. Poisson's ratio is the negative ratio of transverse to axial strain.

determined to be 10 degrees, and stress was measured with each dekyphosis angle from 0 to 10 degrees. As shown in the postdecompression model with a Cobb angle (the angle formed between a line drawn parallel to the superior endplate of the upper vertebra and a line drawn parallel to the inferior endplate of the lower vertebra) between T7 and T11 of 19 degrees in Figure 5, dekyphosis was reproduced by rotating the upper part of T7 by −5 degrees and the lower part of T11 by 5 degrees (total rotation, 10 degrees).

3. Results

3.1. Analysis of the Model before Posterior Decompression. When the occupation rate of OPLL was gradually increased from 0%, stress in the spinal cord began to develop at about 25%, and it increased with the occupation rate. In particular, when the occupation rate exceeded 60%, the spinal cord was markedly deformed, and stress sharply increased (Figures 6(a) and 7). The maximum stress at an occupation rate of 70% was 618 kPa.

3.2. Analysis of the Model after Posterior Decompression. In the postdecompression model as well as the predecompression model, stress increased with the occupation rate. The stress in this model was similar to that in the predecompression model until an occupation rate of 50%, but it was lower than that in the predecompression model at an occupation rate ≥50% (Figures 6 and 7). The maximum stress at an occupation rate of 70% was 295 kPa, showing a 52.3% reduction compared with the value (618 kPa) in the predecompression model.

3.3. Analysis of Dekyphosis. In the model after posterior decompression, dekyphosis reduced stress in the spinal cord. The degree of this reduction increased with an increase in the dekyphosis angle. At an occupation rate of 70%, the stress before dekyphosis (dekyphosis angle was 0 degree) was 295 kPa, but it maximally decreased to 252 kPa (a 14.6% reduction) when the dekyphosis angle was 10 degrees (Figure 8).

4. Discussion

We have reported that posterior decompression followed by kyphosis correction is effective against myelopathy due to thoracic OPLL based on clinical results. However, there have been no mechanical studies on this surgery. In this study, FEMs of thoracic OPLL were produced, and stress generated in the spinal cord was analyzed.

In the predecompression model, stress generated in the spinal cord began to increase when the OPLL occupation rate increased to 25%. This may have been because of contact between OPLL and the spinal cord at an occupation rate of 25%. The maximum stress began to sharply increase at an occupation rate of 60%. The spinal cord comes into contact with the ligamentum flavum at an occupation rate of 50%, but since the ligamentum flavum is soft, this ligament may not have affected the maximum stress at an occupation rate from 50% to 60%. These results suggest that the risk of spinal cord disorder increases at an OPLL occupation rate >60%.

At an OPLL occupation rate ≥60%, stress generated in the spinal cord was lower in the postdecompression model than in the predecompression model. At an occupation rate of 70%, the maximum stress generated in the spinal cord was 618 kPa before posterior decompression and 295 kPa after posterior decompression, showing a 52.3% decrease. This may have been because of the absence of anteroposterior trapping of the spinal cord due to laminectomy. Posterior decompression markedly decreased stress in the spinal cord.

On the other hand, the results of the present experiment suggest that stress remains in the spinal cord even after

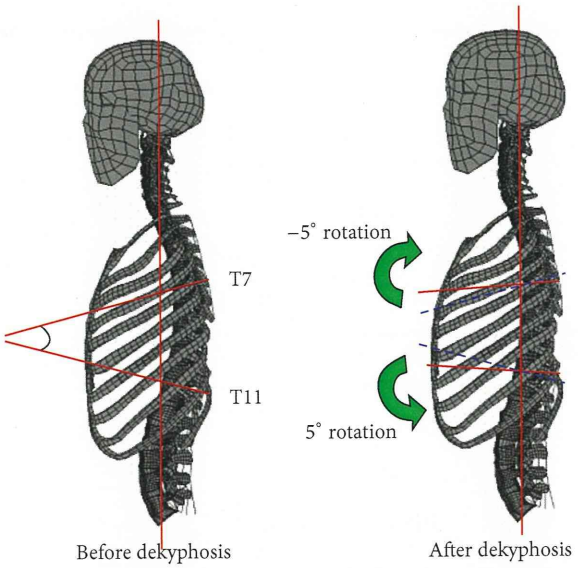

FIGURE 5

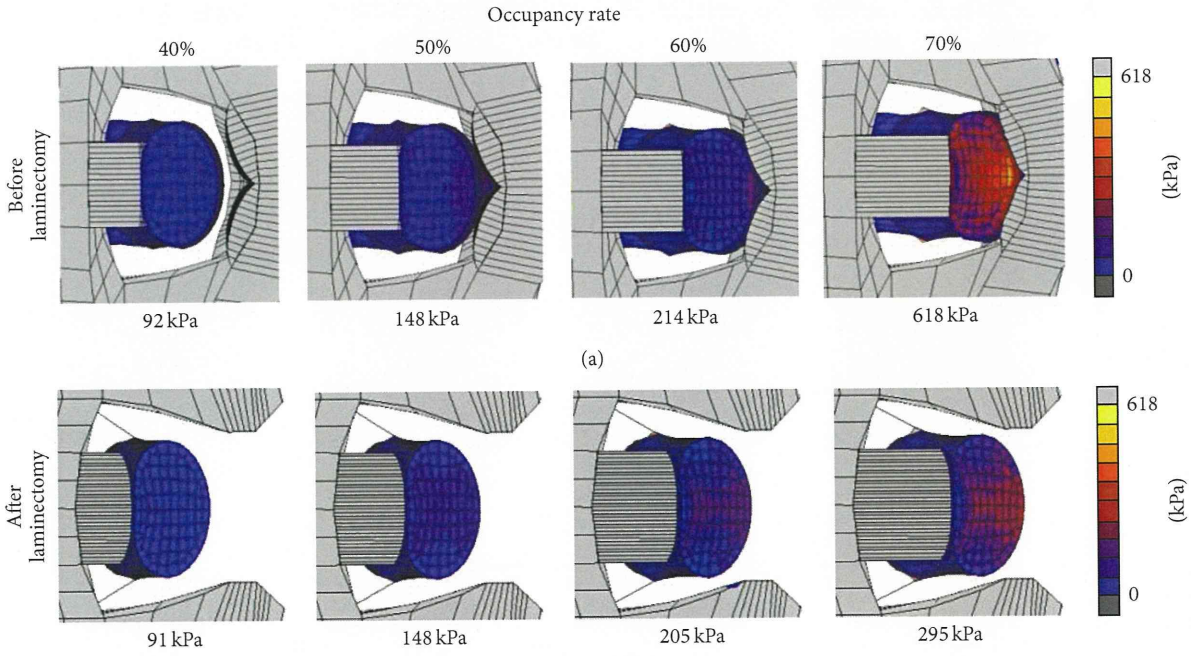

FIGURE 6

posterior decompression, and the effects of posterior decompression performed alone are inadequate in the presence of extensive OPLL. Tokuhashi et al. [15] described that spinal decompression is inadequate in using posterior decompression and fusion alone when the thoracic kyphosis angle is >23 degrees. Ito et al. [16] defined the local ossification angle (the medial angle at the intersection between a line from the superior posterior margin at the cranial vertebral body of maximum OPLL to the top of OPLL with beak type and a line from the lower posterior margin at the caudal vertebral body of the maximum OPLL to the top of OPLL with beak type) and reported poor improvement in the JOA score after posterior decompression alone when this angle was >28 degrees. Thus, since there is a possibility that the results of posterior decompression are affected by not only the size of the anterior ossification lesion but also the local kyphosis angle, changes in stress in the spinal cord after reducing kyphosis were evaluated in the dekyphosis model in this study. As a result,

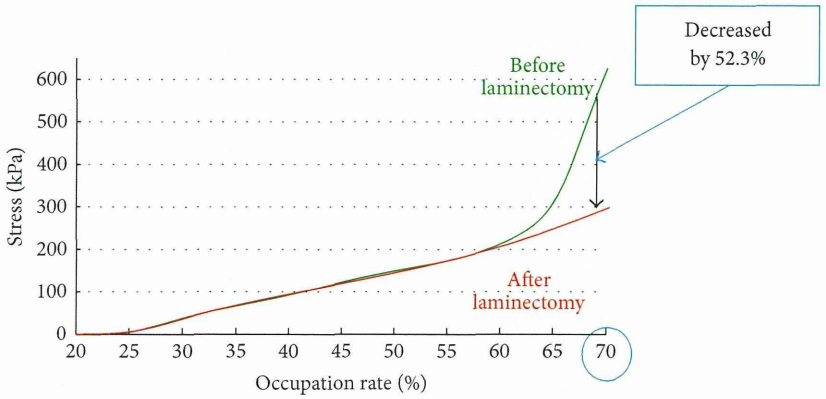

FIGURE 7

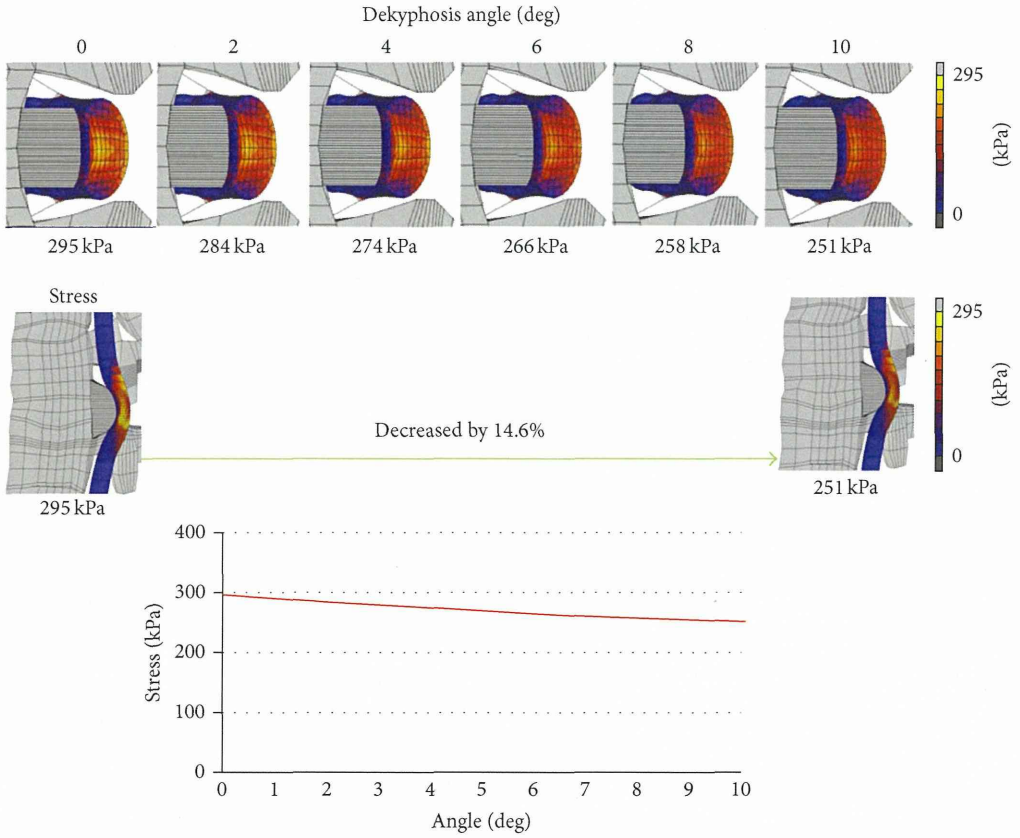

FIGURE 8

the maximum stress decreased by 14.6% after a 10-degree reduction in kyphosis compared with the predekyphosis value in the model at an OPLL occupation rate of 70%. This shows a decrease in spinal cord compression by OPLL after dekyphosis, which may have been because the spinal cord shifted posteriorly after dekyphosis and was indirectly decompressed. Based on these results, further improvement in symptoms by indirect decompression using dekyphosis can be also expected in clinical practice. Matsuyama et al. [17] clearly showed, using intraoperative ultrasonography, a reduction in pressure from OPLL after dekyphosis using posterior instrumentation. Posterior stabilization with instrumentation prevents postoperative kyphosis and the instability after posterior decompression for thoracic OPLL [15, 17–19]. Dekyphosis stabilization is not only to maintain spinal stability but also to reduce the compressive pressure of the OPLL plaque on the spinal cord [3].

In actual surgery, posterior decompression with dekyphosis is performed as a first-step operation, and resection of OPLL using an anterior approach is performed as a second-step operation. Our results showed that stress in the spinal cord is markedly reduced by posterior decompression and

further reduced by the following dekyphosis as a first-step operation. This spinal cord decompression allows safer OPLL resection using an anterior approach as a second-step operation.

In this study, the spinal cord was modeled as a simple shape with a constant thickness. For more detailed analysis of the spinal cord closer to that in the human body, analysis using models that also have the dura meter, cerebrospinal fluid, and internal structures of the spinal cord is necessary. In addition, since the morphology of the spinal cord as well as OPLL differs among individuals, analysis using a model of each patient is also clinically required. Thus, analysis using models closer to the human body is necessary in the future.

5. Conclusion

We reconstructed the OPLL model using a finite element model, and the mechanical stress on the spinal cord was measured.

(1) After the laminectomy when the occupancy rate was 70%, the stress put on the spinal cord is decreased by 52.3%

(2) We found that laminectomy was more effective when the OPLL occupancy rate was greater.

(3) When the dekyphosis angle was 10 degrees, the stress on the spinal cord decreased by 14.6%.

(4) This study demonstrates that the pressure on the spinal cord is indirectly reduced by dekyphosis.

References

[1] K. Tomita, N. Kawahara, H. Baba, Y. Kikuchi, and H. Nishimura, "Circumspinal decompression for thoracic myelopathy due to combined ossification of the posterior longitudinal ligament and ligamentum flavum," *Spine*, vol. 15, no. 11, pp. 1114–1120, 1990.

[2] N. Kawahara, K. Tomita, H. Murakami et al., "Circumspinal decompression with dekyphosis stabilization for thoracic myelopathy due to ossification of the posterior longitudinal ligament," *Rinshou Seikeigeka*, vol. 41, no. 1, pp. 383–388, 2006.

[3] N. Kawahara, K. Tomita, H. Murakami et al., "Circumspinal decompression with dekyphosis stabilization for thoracic myelopathy due to ossification of the posterior longitudinal ligament," *Spine*, vol. 33, no. 1, pp. 39–46, 2008.

[4] N. Tsuzuki, "The section area of vertebral foramen and the figure of spine," *Orthopaedic and Trauma Surgery*, vol. 24, pp. 165–173, 1981.

[5] M. B. Carpenter and J. Sutin, *Carpenter's Neuroanatomy*, Nishimurashoten, Nigata, Japan, 8th edition, 1995.

[6] K. Ozawa, S. Kokubun, and T. Ohasi, "Measurement of mechanical properties of spinal cord by pipette method," *Journal of the Japanese Orthopaedic Association*, vol. 70, p. S1563, 1996.

[7] K. Ichihara, T. Taguchi, I. Sakuramoto, S. Kawano, and S. Kawai, "Mechanism of the spinal cord injury and the cervical spondylotic myelopathy: new approach based on the mechanical features of the spinal cord white and gray matter," *Journal of Neurosurgery*, vol. 99, no. 3, pp. 278–285, 2003.

[8] L. E. Bilston and L. E. Thibault, "The mechanical properties of the human cervical spinal cord in vitro," *Annals of Biomedical Engineering*, vol. 24, no. 1, pp. 67–74, 1996.

[9] J. Scifert, K. Totoribe, V. Goel, and J. Huntzinger, "Spinal cord mechanics during flexion and extension of the cervical spine: a finite element study," *Pain Physician*, vol. 5, no. 4, pp. 394–400, 2002.

[10] F. Barney and P. T. LeVeau, *Biomechanics of Human Motion*, pp. 299–304, W.B. Saunders, Philadelphia, Pa, USA, 3rd edition, 1992.

[11] K. Ono, H. Ota, and K. Tada, "Ossified posterior longitudinal ligament: a clinicopathologic study," *Spine*, vol. 2, no. 2, pp. 126–138, 1977.

[12] G. Nishiura, M. Koyama, and H. Handa, "Clinical consideration of 182 patients with ossification of the longitudinal ligament of the cervical spine," *Spinal Code*, vol. 7, pp. 1021–1028, 1994.

[13] T. Nose, T. Egashira, and T. Enomoto, "Ossification of the posterior longitudinal ligament: a clinico-radiological study of 74 cases," *Journal of Neurology Neurosurgery and Psychiatry*, vol. 50, no. 3, pp. 321–326, 1987.

[14] S. Matsunaga, T. Sakou, and K. Hayashi, "Trauma-induced myelopathy in patients with ossification of the posterior longitudinal ligament," *Journal of Neurosurgery*, vol. 97, no. 2, pp. 172–175, 2002.

[15] Y. Tokuhashi, H. Matsuzaki, and M. Hoshino, "Effectiveness of posterior decompression for patient with ossification of the posterior longitudinal ligament in the thoracic spine. Usefulness of the Ossification-Kyphosis angle on MRI," *Spine*, vol. 31, no. 1, pp. E26–E30, 2006.

[16] K. Ito, Y. Yukawa, Y. Horie, and F. Kato, "Surgical treatment for ossification of posterior longitudinal ligament in thoracic spine. Influence of local ossification angle," *Rinshou Seikeigeka*, vol. 43, pp. 539–542, 2008.

[17] Y. Matsuyama, H. Yoshihara, T. Tsuji et al., "Surgical outcome of ossification of the posterior longitudinal ligament (OPLL) of the thoracic spine: implication of the type of ossification and surgical options," *Journal of Spinal Disorders and Techniques*, vol. 18, no. 6, pp. 492–497, 2005.

[18] M. Yamazaki, A. Okawa, M. Koda, S. Goto, S. Minami, and H. Moriya, "Transient paraparesis after laminectomy for thoracic myelopathy due to ossification of the posterior longitudinal ligament: a case report," *Spine*, vol. 30, no. 12, pp. E343–E346, 2005.

[19] M. Yamazaki, M. Koda, A. Okawa, and A. Aiba, "Transient paraparesis after laminectomy for thoracic ossification of the posterior longitudinal ligament and ossification of the ligamentum flavum," *Spinal Cord*, vol. 44, no. 2, pp. 130–134, 2006.

PLOS ONE

The Prevalence and Phenotype of Activated Microglia/Macrophages within the Spinal Cord of the Hyperostotic Mouse (*twy/twy*) Changes in Response to Chronic Progressive Spinal Cord Compression: Implications for Human Cervical Compressive Myelopathy

Takayuki Hirai[1], Kenzo Uchida[1]*, Hideaki Nakajima[1], Alexander Rodriguez Guerrero[1], Naoto Takeura[1], Shuji Watanabe[1], Daisuke Sugita[1], Ai Yoshida[1], William E. B. Johnson[2], Hisatoshi Baba[1]

1 Department of Orthopaedics and Rehabilitation Medicine, Faculty of Medical Sciences, University of Fukui, Eiheiji, Fukui, Japan, **2** Life & Health Sciences, Aston University, Aston Triangle, Birmingham, United Kingdom

Abstract

Background: Cervical compressive myelopathy, e.g. due to spondylosis or ossification of the posterior longitudinal ligament is a common cause of spinal cord dysfunction. Although human pathological studies have reported neuronal loss and demyelination in the chronically compressed spinal cord, little is known about the mechanisms involved. In particular, the neuroinflammatory processes that are thought to underlie the condition are poorly understood. The present study assessed the localized prevalence of activated M1 and M2 microglia/macrophages in *twy/twy* mice that develop spontaneous cervical spinal cord compression, as a model of human disease.

Methods: Inflammatory cells and cytokines were assessed in compressed lesions of the spinal cords in 12-, 18- and 24-weeks old *twy/twy* mice by immunohistochemical, immunoblot and flow cytometric analysis. Computed tomography and standard histology confirmed a progressive spinal cord compression through the spontaneously development of an impinging calcified mass.

Results: The prevalence of CD11b-positive cells, in the compressed spinal cord increased over time with a concurrent decrease in neurons. The CD11b-positive cell population was initially formed of arginase-1- and CD206-positive M2 microglia/macrophages, which later shifted towards iNOS- and CD16/32-positive M1 microglia/macrophages. There was a transient increase in levels of T helper 2 (Th2) cytokines at 18 weeks, whereas levels of Th1 cytokines as well as brain-derived neurotrophic factor (BDNF), nerve growth factor (NGF) and macrophage antigen (Mac) −2 progressively increased.

Conclusions: Spinal cord compression was associated with a temporal M2 microglia/macrophage response, which may act as a possible repair or neuroprotective mechanism. However, the persistence of the neural insult also associated with persistent expression of Th1 cytokines and increased prevalence of activated M1 microglia/macrophages, which may lead to neuronal loss and demyelination despite the presence of neurotrophic factors. This understanding of the aetiopathology of chronic spinal cord compression is of importance in the development of new treatment targets in human disease.

Citation: Hirai T, Uchida K, Nakajima H, Guerrero AR, Takeura N, et al. (2013) The Prevalence and Phenotype of Activated Microglia/Macrophages within the Spinal Cord of the Hyperostotic Mouse (*twy/twy*) Changes in Response to Chronic Progressive Spinal Cord Compression: Implications for Human Cervical Compressive Myelopathy. PLoS ONE 8(5): e64528. doi:10.1371/journal.pone.0064528

Editor: Michelle L. Block, Virginia Commonwealth University, United States of America

Received January 12, 2013; **Accepted** April 16, 2013; **Published** May 24, 2013

Funding: This study was supported by Grants-in-Aid to HB and KU for General Scientific Research of the Ministry of Education, Science and Culture of Japan (#B-22390287 and #B-24390351) and also by grants to HB and KU from the Investigation Committee on Ossification of the Spinal ligaments, Public Health Bureau of the Japanese Ministry of Health and Welfare (2011–2014). The funders had no role in study design, data collection and analysis, decision to publish, or preparation of the manuscript.

Competing Interests: The authors have declared that no competing interests exist.

* E-mail: kuchida@u-fukui.ac.jp

Introduction

Mechanical compression of the spinal cord can cause neural tissue damage, reduction of neuronal cell activity and protein synthesis, and neuronal cell death. Cervical compressive myelopathy is characterized by progressive stenosis of the cervical canal and compression of the spinal cord due to spondylosis, degenerative disc disease, and ossification of the posterior longitudinal ligament (OPLL) [1–4]. Symptoms usually start to appear after middle age with slowly progressive clumsiness and paresthesia in the hands, gait disturbance, and signs of posterior and pyramidal column dysfunction; eventually leading to tetraplegia or tetraparesis. Human pathological studies have reported flattening of the anterior horns, loss of anterior horn cells, cavity formation,

ascending demyelination in the posterior columns, descending demyelination in the lateral columns and proliferation of hyalinized small blood vessels [5–7]. However, since it is difficult to properly estimate and follow the progression of these changes in humans, considerable uncertainty exists regarding the biological and molecular mechanisms responsible for the demyelination that takes place in these disorders, and for the progressive loss of neurons and oligodendrocytes. Moreover, although pro-inflammatory cytokines and related immune effector molecules are considered to be produced after chronic, slow compression of the spinal cord as seen in cervical compressive myelopathy, and could result in induction of cell death through necrosis and apoptosis, their role in compression-induced damage remain questionable [8,9].

The inflammatory changes following spinal cord injury (SCI) are complex and involve the activation of resident microglia and recruitment of neutrophils, macrophages and lymphocytes into the lesion from the systemic circulation [10–12]. This leads to tissue damage, demyelination and neurological dysfunction [13], as well as apoptosis of neurons and oligodendrocytes [14,15]. Activated microglia and recruited macrophages (which are antigenically not distinguishable, henceforth these cell types have been referred to as microglia/macrophages) are implicated in neuroinflammation through the induction or modulation of a broad spectrum of cellular responses [10]. These cells are the primary source for pro-inflammatory cytokines within the spinal cord, and their presence and activity have the potential to act as markers of disease onset and prognosis of neurological outcome following SCI [13,16]. Interestingly such neuroinflammation, including the microglial response, has also been identified as a contributor to cell death in ischemic injury in the brain [17] and chronic neurodegenerative disorders [18]. These findings point to the potential commonality of mechanisms underlying cell damage and cell death in both acute neural injury and in slow-developing pathologies of neural systems, like those seen in Alzheimer's disease and Parkinson disease, even in the absence of prominent leukocyte infiltration [18].

Recent studies have demonstrated phenotypic changes in macrophages during the immunological and inflammatory responses to various conditions [19,20]. This divergence is referred to as macrophage polarization and has been reported in non-neural [21] and neural tissues [22,23], and also in both *in vitro* and *in vivo* experiments [24]. Approximately, two subtypes of macrophages have become of great interest in the field of spinal cord regeneration: classically activated macrophages (M1 phenotype) and alternatively activated macrophages (M2 phenotype) [25–28]. Whereas the M1 phenotype is the product of exposure to T helper 1 (Th1) cytokines, such as interferon gamma (IFN-γ), tumor necrosis factor-alpha (TNF-α), and interleukin (IL)-6, the M2 phenotype is activated via T helper 2 (Th2) cytokines, such as IL-4, IL-10, and IL-13 [22,29,30]. While the M1 phenotype is known for their high expression of inflammatory cytokines and bactericidal activity, M2 phenotype exhibits enhanced phagocytic and anti-inflammatory properties; although at least three subsets of M2 macrophages have also been documented [21,25]; for such reasons, macrophages with the latter phenotype are considered to function in recovery of SCI [19,23,31]. Thus, modification of the SCI microenvironment to increase the number of M2 macrophages may promote neuroprotection. A similar possibility has also been recently attributed to microglia by showing that these cells can also be induced under certain conditions to both extremes of the M1 and M2 differentiation spectrum [25,32].

The study of the pathological mechanisms of spinal cord dysfunction related to cervical spondylotic myelopathy (CSM) and OPLL has been impaired in the past due to the lack of good *in vivo* models. However, this has changed with the recent characterization of the tip-toe Walking Yoshimura (*twy/twy*) mouse; an autosomal recessive mutant. The *twy/twy* mouse has a spontaneous mutation in the nucleotide pyrophosphatase (*Npps*) gene developing posterior calcification of the atlantoaxial membrane at the cervical (C) 1-C2 vertebral level. The defective vertebral column causes cervical spinal cord compression progressively over several months. Thus, our group has used the *twy/twy* mouse as a suitable model to investigate the effects of the chronic, slow compression of the spinal cord that is seen in CSM and OPLL [33–36].

Recent studies have suggested that neuronal and oligodendrocytic apoptosis through activation of the Fas death receptor pathway is a key event in the *twy/twy* mouse spinal cord [37] and have shown that neutralization of Fas ligand with a function-blocking antibody reduced neural inflammation at the lesion mediated by activated microglia and macrophages [7]. Another study from our laboratory reported that increased expression of TNF-α and TNF receptor 1 (TNFR1) released by the activated microglia/macrophages correlated with neuronal and oligodendrocytic apoptosis [8]. Based on the above findings, the present study was designed to provide insight on previously unexplored aspects of microglia/macrophage phenotypic changes induced by chronic, slow spinal cord compression seen in cervical compressive myelopathy. Specially, we investigated the expression and colocalization of markers of microglia/macrophages (both M1 and M2 phenotypes) as well as the levels of neuroinflammatory cytokines closely related to these cells, which could promote neurotoxicity or neuroprotection and lesion repair in the *twy/twy* spinal cord.

Materials and Methods

The Spinal Hyperostotic *twy/twy* and Control Mice and Spinal Cord Progressive Compression Evaluated by Computed Tomography (CT)

The Ethics Review Committee for Animal Experimentation of University of Fukui approved the experimental protocol. Spinal hyperostotic *twy/twy* mice purchased from the Central Institute for Experimental Animals (Kawasaki, Japan), were used in all experiments (aged 12 weeks; n = 29, 18 weeks; n = 29, 24 weeks; n = 29) (Table S1). Homozygous *twy/twy* mice were maintained by brother-sister mating of heterozygous Institute of Cancer Research (ICR) mice (+/*twy*). ICR mice at the age of 12, 18, and 24 weeks were used as control animals (n = 10 in each age group). The disorder is inherited in an autosomal recessive manner and the homozygous hyperostotic mouse is identified by a characteristic tip-toe walking at 6 to 8 weeks of age, but no congenital neurological abnormalities are detected at that age. The *twy/twy* mouse exhibits spontaneous calcified deposits posteriorly at the C1–C2 vertebral level, producing a variable degree of compression of the spinal cord between C2 and C3 cord segments with a general ankylosis of joints. The calcified mass grows in size progressively with age particularly in the atlantoaxial membrane, causing profound motor paresis at the age of 18–24 weeks [9,33,37].

For hematoxylin and eosin (H&E) staining, the resected cervical spine of each *twy/twy* mouse of different ages (n = 5 for each time point) was fixed in buffered formaldehyde for 48 hours at 4°C. The sample was then decalcified for 2 weeks at 4°C in 0.5 M ethylenediaminetetraacetic acid (0.5 M Tris-HCl buffer) at pH 7.6 and then embedded in paraffin using standard procedures. Serial 4-μm-thick cryostat sagittal and axial sections were prepared.

In order to confirm differences in the severity of compression before H&E staining, flow cytometry, and immunoblot analysis, we measured the spinal canal area in the cervical spine of *twy/twy* mice on CT scans (GE Medical Systems, Milwaukee, WI) obtained under anesthesia with ravonal (Tiopental®, Mitsubishi Tanabe Pharma, Osaka, Japan), using Image J, the image analysis software of the National Institutes of Health (Bethesda, MD). The correlation between age and spinal canal area at the site of maximum compression at C1–C2 vertebral level was determined. We also compared the spinal canal areas at C1–C2 to that at thoracic (Th) 1 vertebral level. In the same way, we also compared the spinal cord areas at the site of maximum compression in H&E staining at C1–C2 to that at Th1 vertebral level using the color image analyzer (MacSCOPE, Minani, Fukui, Japan).

Immunohistochemistry

Deep anesthesia was induced in each group of mice (n = 5 *twy/twy* mice and n = 2 control ICR mice for axial sections, and n = 2 *twy/twy* mice for sagittal sections in each time point) followed by transcardial perfusion and fixation with 4% paraformaldehyde in 0.1 M phosphate-buffered saline (PBS); the spinal cords were dissected and post-fixed in the same fixative for a few hours. The tissue samples were immersed in 10% sucrose in 0.1 M PBS at 4°C for 24 hours, and 30% sucrose in 0.1 M PBS for 24 hours. Segments of the cervical spinal cord were embedded in optimal cutting temperature compound (Sakura Finetek, Torrance, CA) and cut on a cryostat into serial 10 μm-thick axial or sagittal frozen sections, which were serially mounted on glass slides and fixed with 2% paraformaldehyde in 0.1M PBS for 5 minutes, rinsed in PBS and stored at −80°C.

For immunofluorescence staining, frozen sections were permeabilized with 0.1 M Tris-HCl buffer (pH 7.6) containing 0.3% Triton X-100. The following primary antibodies diluted in Antibody Diluent with Background Reducing Components (Dako Cytomation, Carpenteria, CA) were applied overnight at 4°C: rabbit anti-Integrin αM (equivalent to CD11b), 1:200 (Santa Cruz Biotechnology, Santa Cruz, CA); mouse anti-neuronal nuclei (NeuN) monoclonal antibody, 1:400 (Millipore Corporation, Billerica, MA); rabbit anti-inducible nitric oxide synthase (iNOS), 1:200 (BD Pharmingen, San Jose, CA); rat anti-CD16/32, 1:200 (Santa Cruz Biotechnology); goat anti-arginase-1, 1:200 (Santa Cruz Biotechnology); goat anti-CD206, 1:200 (Santa Cruz Biotechnology); rabbit anti-brain derived neurotrophic factor (BDNF) polyclonal antibody, 1:300 (Abcam plc, Cambridge, UK); rabbit anti-nerve growth factor (NGF) polyclonal antibody, 1:300 (Abcam plc); anti-macrophage antigen-2 (Mac-2), 1:200 (BioLegend, San Diego, CA); and mouse monoclonal anti-CD4 antibody, 1:100 (Abcam plc). The sections were then incubated for 1 hour at room temperature with Alexa Fluor-conjugated 488- or 568- secondary antibodies, 1:250 (Molecular Probes, Eugene, OR). Finally, the sections were washed, wet-mounted, and examined by the omission of a primary antibody or through the use of a non-specific negative primary antibody that was isotype matched. Furthermore, some sections were counterstained with nuclear marker DAPI (Abbott Molecular, Des Plaines, IL).

All images were obtained using a fluorescence microscope (Olympus AX80, Olympus Optical, Tokyo) or a confocal laser scanning microscope (model TCS SP2, Leica Instruments, Nussloch, Germany), where the 488- and 543-nm lines of the argon/helium-neon laser were used for fluorescence excitation.

Semi-quantitative Analysis of Stained Tissues

Changes in CD11b-(red), NeuN- (green) and CD4- (red) positive areas at 12, 18, and 24 weeks of age *twy/twy* mice, and control ICR mice were assessed by the following procedure: serial axial sections were divided into five groups (slide glass) by collecting every fifth section separately from the site of maximum compression (between the C2 and C3 dorsal roots) and half of the spinal cord on the compressed side was analyzed using grain counting with the light intensity automatically set by the color image analyzer (MacSCOPE).

The proportions of CD11b-positive cells double immunostained with iNOS, CD16/32, arginase-1 or CD206 in each groups were determined semi-quantitatively by the following procedure: the serial axial sections divided into five groups (slides) as mentioned above from the site of maximum compression (between the C2 and C3 dorsal roots) and the number of positive cells per cross-section in each fluorescence stain was determined automatically using grain counting based on light intensity by a color image analyzer (MacSCOPE). The light intensity and threshold values were maintained at constant levels when collecting digitized images in all analysis. We documented the extent to which the microglia/macrophages present within the spinal cord were polarized by the M1/M2 ratio, as determined by the number of CD11b cells that were also positive iNOS and CD16/32/the number of CD11b cells that were also positive for CD206 and arginase-1.

Flow Cytometry

Immediately after deep anesthesia, the mouse was perfused intracardially with 200 ml of ice-cold 0.1 M PBS, and the spinal cords were harvested (n = 3 for each time point). The cervical spinal cord around the maximally compressed site was surgically dissected and dissociated with collagenase, 175 U/ml (Sigma-Aldrich, St. Louis, MO) for 1 hour at 37°C. Cells were washed in Dulbecco's modified Eagle's Medium (Invitrogen Life Technologies, Carlsbad, CA) containing 10% fetal bovine serum and filtered through a 40 μM nylon cell strainer (BD Biosciences, San Jose, CA) under centrifugation to remove tissue debris and obtain a single-cell suspension, as described in detail previously [38].

From this point on, prior to every staining, a cell-count was performed in every sample to ensure a cell density of 1.0×10^6 cells/100 μL. Cells were incubated for 1 hour on ice with the following fluorescent antibodies: allophycocyanin (APC) rat anti-CD45, 0.25 μg/ml (BioLegend, San Diego, CA); Pacific Blue rat anti-Ly-6G/Ly-6C, 1.0 μg/ml (equivalent to Gr-1; BioLegend) and PerCP-Cy 5.5 rat anti-CD11b, 0.25 μg/ml (BD Pharmigen, San Jose, CA). For intracellular staining [39], the cells were resuspended in Fixation buffer and treated with Permeabilization Buffer (both from Santa Cruz Biotechnology) followed by re-suspension in ice-cold PBS and incubation for 1 hour with goat anti-arginase 1, 1:200 conjugated to fluorescein isothiocyanate (FITC),1:200 (Santa Cruz Biotechnology) and phycoerythrin (PE)-conjugated rabbit anti-iNOS, 3.0 μg/ml (Abcam plc); or PE/Cy7 conjugated rat anti-CD16/32, 1.0 μg/ml (Biolegend) and FITC rat anti-CD206, 1.0 μg/ml (Biolegend). Samples with cells alone were used as negative controls to eliminate background autofluorescence, and samples where the cells had been incubated with a single-added antibody were used as positive controls to set up the cytometer alignment and to remove any spectral overlap.

Flow cytometry was performed immediately using a FACS Canto™ II (Becton Dickinson Biosciences, San Jose, CA). Forward scatter was set to further eliminate any cellular debris from analysis. In each test, a minimum of 250,000 cells were analyzed and the data were processed using BD FACSDiva software (Becton Dickinson Biosciences). The different cell populations present in the suspension were classified according to the combination of expressed antigens, as stated in previous

reports, as follows: $CD11b^{high}/CD45^{low}/GR\text{-}1^{negative}$ represented resting microglia [39], and $CD11b^{high}/CD45^{high}/GR\text{-}1^{negative}$ represented activated microglia/macrophages [38]. At the previously described time points, $CD11b^{high}$ cells in the spinal cord were sub-fractioned into a $CD45^{low}/GR\text{-}1^{negative}$ population, identifying them as resting microglia. In a similar fashion, $CD11b^{high}$ cells were sub-fractioned into a $CD45^{high}/GR\text{-}1^{negative}$ population, which identified them as activated microglia/macrophages.

The phenotype of microglia/macrophage sub-populations was corroborated through their expression of iNOS or CD16/32 (pro-inflammatory M1 phenotypes) as well as arginase 1 and CD206 (anti-inflammatory M2 phenotypes).

Myeloperoxidase (MPO) Staining and Assay

The 3,3′-diaminobenzidine (DAB) staining kit (Muto Pure Chemicals Co., Tokyo) was used in each mouse (n = 3 for each time point) for cytochemical staining of MPO according to the instructions supplied by the manufacturer. Briefly, the peroxidase reaction was developed with 0.05% 3,3′-DAB in 50 mmol/L Tris-HCl (pH 7.6) and 0.03% H_2O_2 for 1 to 2.5 min. The sections were counterstained with eosin, dehydrated, and mounted. Oxidized 3,3′- DAB (a brown, highly insoluble indamine polymer) was visible under light microscopy.

MPO activity levels in harvested compressed spinal cord tissues (n = 3 for each time point) were measured with MPO assay kit (BioVision, Milpitas, CA) using a spectrophotometer at 412 nm. One unit of MPO activity was defined as the amount of enzyme degrading 1 μmol of 5-thio-2-nitrobenzoic acid (TNB) per minute at 25°C. MPO activities in the spinal cord tissues were calculated by using a standard curve generated with MPO and expressed in units per miligram weight of wet tissue.

Immunoblot Analysis

Immediately after deep anesthesia, the spinal cord of each mouse (n = 3 for each time point) around the maximally compressed site (between C2 and C3 dorsal roots) was carefully dissected *en bloc* from the cervical spine and stored immediately at −80°C in liquid nitrogen. Segments were centrifuged at 15,000×*g* for 30 seconds using a BioMasher Rapid Homogenization Kit (Funakoshi, Tokyo), then solubilized in RIPA lysis buffer 1X (Santa Cruz Biotechnology), homogenized and stored at −80°C. The protein concentration was determined in the obtained samples by a Lowry protein Assay using a DC protein assay kit (Bio-Rad Laboratories, Hercules, CA). Laemmli sodium dodecyl-sulfate buffer samples containing the protein mixtures were boiled and subjected to immunoblot analysis. Total protein (20 μg/lane) was separated on 12.5% SDS-PAGE and transferred onto polyvinylidene difluoride membrane (PE Applied Biosystems, Foster, CA) for 70 minutes using a semi-dry blot apparatus. The membrane was washed twice in PBS containing 0.05% Tween 20, blocked by 5% skimmed milk in PBS for 1 hour at room temperature, and then incubated with one of the following antibodies: rabbit anti- IFN-γ, 0.2 μg/ml (Abcam plc), rabbit anti-TNF-α, 0.2 μg/ml (Abcam plc), rabbit anti- IL-6, 1:200 (Santa Cruz Biotechnology), rat anti-IL-4, 1:200 (Santa Cruz Biotechnology), rabbit anti-IL-10, 1:200 (Santa Cruz Biotechnology), goat anti-IL-13, 1:200 (Santa Cruz Biotechnology), rabbit anti-BDNF, 1:200 (Abcam plc), rabbit anti-NGF, 1:200 (Abcam plc), or rat anti-Mac-2, 1:200 (BioLegend) overnight at 4°C. After triple washing in 0.1 M PBS, the membranes were incubated for 1 hour in the respective secondary IgG/HRP complex antibodies: anti-goat, 1:1,000; anti-rabbit, 1:5,000; or anti-rat, 1:1,000 (all from Santa Cruz Biotechnology). After triple washing with 0.1 M PBS, the membrane was immersed in ECL Advance Western Blot Detection kit (GE Healthcare, Buckinghamshire, UK) for 1 minute and then exposed to X-ray film for visualization of peroxidase activity and determination of the level of each specific protein. The band intensities were normalized to β-actin, 1:2000 (Abcam plc), and Kaleidoscope Prestained Standards (Bio-Rad Laboratories) was used as the molecular weight control.

Statistical Analysis

All values are expressed as mean± standard deviation (SD). Differences between groups were examined for statistical significance using one-way factorial analysis of variance (ANOVA). Before the priori comparison, Kolmogorov-Smirnov test was used for verification of normality. A p value <0.05 denoted the presence of a significant difference with Tukey's post hoc analysis. The above tests were conducted using SPSS software version 11.0 (SPSS, Chicago, IL).

Results

Chronic and Slow Progressive Compression in *twy/twy* Mouse Induces the Increase of Activated Microglia/Macrophages

The *twy/twy* mouse exhibited a clear age-related compression of the spinal cord at the C1–C2 vertebral level. The calcified mass grew progressively with age particularly in the atlantoaxial membrane posteriorly at the C1–C2 vertebral level (Figs. 1A–D). CT scans and H&E staining demonstrated that the spinal canal and spinal cord transverse area rate at the C1–C2 relative to that at the Th1 vertebral level was 0.902±0.077 and 0.795±0.098 in 12-week-old, 0.677±0.162 and 0.623±0.151 in 18-week-old, 0.423±0.107 and 0.397±0.101 in 24-week-old *twy/twy* mice, respectively (Figs. 1B–G). These results indicated there is correlation between the CT findings and histological examinations, and that the spinal canal and spinal cord transverse area decreased with advancing age.

The area of the spinal cord that was positive for CD11b immunostained increased and that area which was positive for NeuN immunostained cells decreased with advancement of spinal cord compression. The CD11b-positive area increased according to the degree of spinal cord compression in both the gray and white matters, especially in the anterior horn and anterior column of the maximally compressed site compared with the rostral or caudal sites of the spinal cord (Fig. 2A). On the other hand, the NeuN-positive area, mainly in the anterior horn, decreased accordingly to the degree of spinal cord compression; the difference between 18- and 24-week-old *twy/twy* mice was significant (Fig. 2). The results of ICR mice in each age group (12-, 18-, and 24-week-old) were the same as those from 12-week-old *twy/twy* mice (Fig. S1A).

Chronic Progressive Spinal Cord Compression Induces Changes in the Phenotype Markers of Microglia/Macrophages

To evaluate the phenotype of microglia/macrophages, tissues were immunostained with iNOS and CD16/32 for the M1 phenotype, and arginase-1 and CD206 for the M2 phenotype, as well as the pan-specific marker CD11b for microglia/macrophages. Double-positive merged cells were found particularly in the anterior horn and anterior column. In control ICR mice (with the same results seen in each age group; Fig. S1B) and in 12-week *twy/twy* mice, multiple cells co-expressing arginase-1 and CD11b were found; but no CD11b-positive cells co-expressing iNOS, CD16/32

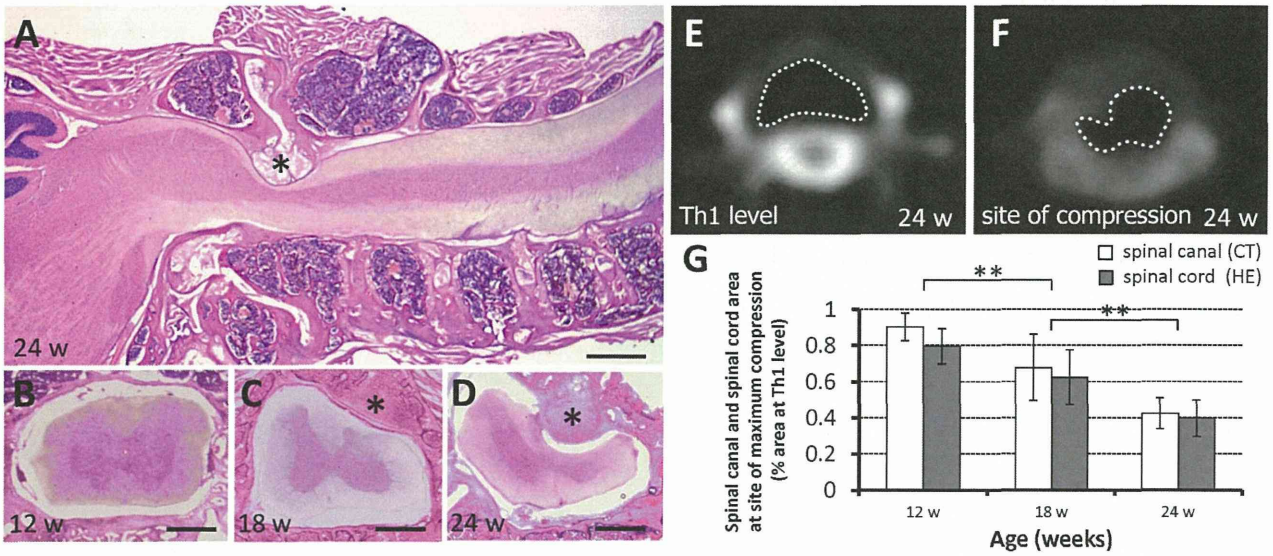

Figure 1. Histological and imaging evidence of progressive cervical spinal compression in *twy/twy* mice. Microphotographs of hematoxylin and eosin (H&E)-stained sagittal (A) and transaxial (B–D) sections, and computed tomography (CT) scans (E, F) of the cervical spine of 12- (B), 18- (C) and 24-week-old *twy/twy* mice (A, D, E, F). Calcified lesions originating from the atlantoaxial membrane increased in size progressively with age, compressing the lateral and dorsal aspects of the spinal cord between C2 and C3 segments (*) calcified lesions. A spinal canal transverse area on CT at thoracic (Th) 1 level and the site of compression of a 24-week-old *twy/twy* mouse is surrounded by white dotted line in (E, F). The relative spinal canal and spinal cord transverse area was shown compared with that of Th1 vertebral level assessed by CT and H&E staining (G). The spinal canal and spinal cord transverse area decreased with advancing age. Scale bars = 500 μm (A); 200 μm (B–D). **p<0.01 (n = 3 for each time point).
doi:10.1371/journal.pone.0064528.g001

or CD206 were identified (Fig. 3A). In 18-week *twy/twy* mice, while some CD11b-positive cells co-expressed iNOS or CD16/32, the number of those co-expressing arginase-1 or CD206 and CD11b remained higher (Fig. 3B). In 24-week *twy/twy* mice, while the number of CD11b- positive cells co-expressing iNOS or CD16/32 remained elevated, that of cells co-expressing CD11b and arginase-1 or CD206 persisted as the most abundant type (Fig. 3C). These differences between iNOS-CD16/32 and arginase-1-CD206 were statistically significant in 18- and 24-week-old *twy/twy* mice (Fig. 3D). Figure 3E shows the antigen expression ratio of M1 phenotype (CD11b-positive cells co-expressing iNOS or CD16/32)/M2 phenotype (CD11b-positive cells co-expressing arginase-1 or CD206) using immunofluorescence staining. The percentage of microglia/macrophages that was of M2 phenotype was 82.0% in 18-week-old and 61.6% in 24-week-old *twy/twy* mice with a concomitant increase in the percentage of microglia/macrophages that were of M1 phenotype.

To further determine the activity of CD11b-positive cells in the chronically compressed spinal cords, the profile of the CD11b-positive cells was analyzed by flow cytometry (Fig. 4). Of the 250,000 spinal cord cells, 10.4±0.7% (26,041±1,794 cells) was CD11b ^{positive}. The immunoprofile of CD11b-positive cells shifted from CD11b^{high}/CD45^{low}/GR-1^{negative} cells (resting microglia) to CD11b^{high}/CD45 ^{high}/GR-1^{negative} cells (activated microglia/macrophages) with the advancement of spinal cord compression (Figs. 4A–C). While almost all CD11b-positive cells were resting microglia in control ICR mice (with the same results seen in each age group; Fig. S2A) and in 12-week *twy/twy* mice, the population of activated microglia/macrophages increased significantly in the 18- and 24-week *twy/twy* mice (Figs. 4D and E).

We also determined the subtypes of resting microglia and activated microglia/macrophages in terms of M1/M2 phenotypic marker expression (Fig. 5). Of the CD11b^{high}/CD45 ^{low}/GR-1^{negative} cells (resting microglia), 10.2±2.2% (458±97 cells) in 12-week and 73.0±16.1% (4017±884 cells) in 18-week-old *twy/twy* mice were arginase-1 ^{positive}, while only a few were iNOS ^{positive}, CD16/32 ^{positive} or CD206 ^{positive}. The number of arginase-1 ^{positive} resting microglia in samples from control ICR mice of each age group were the same as in 12-week-old *twy/twy* mice (Fig. S3). Of the CD11b^{high}/CD45 ^{high}/GR-1^{negative} cells (activated microglia/macrophages), 5.1±1.1% (531±112 cells) were iNOS ^{positive}, 7.6±1.5% (788±156 cells) were arginase-1 ^{positive}, 23.7±5.2% (2577±564 cells) were CD16/32 ^{positive} and 56.3±12.5% (6123±1358 cells) were CD206 ^{positive} in the 18 week *twy/twy* mice (Fig. 5B). In the activated microglia/macrophages in the 24-week *twy/twy* mice, 30.9±1.4% (3205±150 cells), 44.2±8.9% (4578±925 cells), 43.6±9.3% (4851±1032 cells), and 48.9±11.0% (5442±1223 cells) were iNOS ^{positive}, arginase-1 ^{positive}, CD16/32 ^{positive} and CD206 ^{positive}, respectively (Fig. 5C). These results indicated that the prevalence of microglia/macrophages of M2 phenotype (arginase-1 and CD206) remained dominant compared to that of the M1 phenotype (iNOS and CD16/32), despite the advancement of spinal cord compression, in agreement with the results of immunostaining. In some of these dot plots, a proportion of microglia/macrophages were double positive to M1 (CD16/32) and M2 (CD206) phenotypic markers (<15%).

M2 Microglia/Macrophages are a Source of Neurotrophic Factors in the Chronically Compressed Spinal Cord

To evaluate the expression of neurotrophic factors and phagocytic activity in correlation with M1 and M2 phenotypes, double immunofluorescence staining for BDNF, NGF, and Mac-2 with either iNOS or arginase-1 was performed. Double-positive cells were found particularly in the anterior horn and anterior column. In 12-week *twy/twy* mice, some expression of BDNF, NGF and no expression of Mac-2 was found (Fig. 6A): those expressions were also noted in 18-week-old *twy/twy* mice (Fig. 6B) and their intensity reached peak levels in 24-week-old *twy/twy* mice

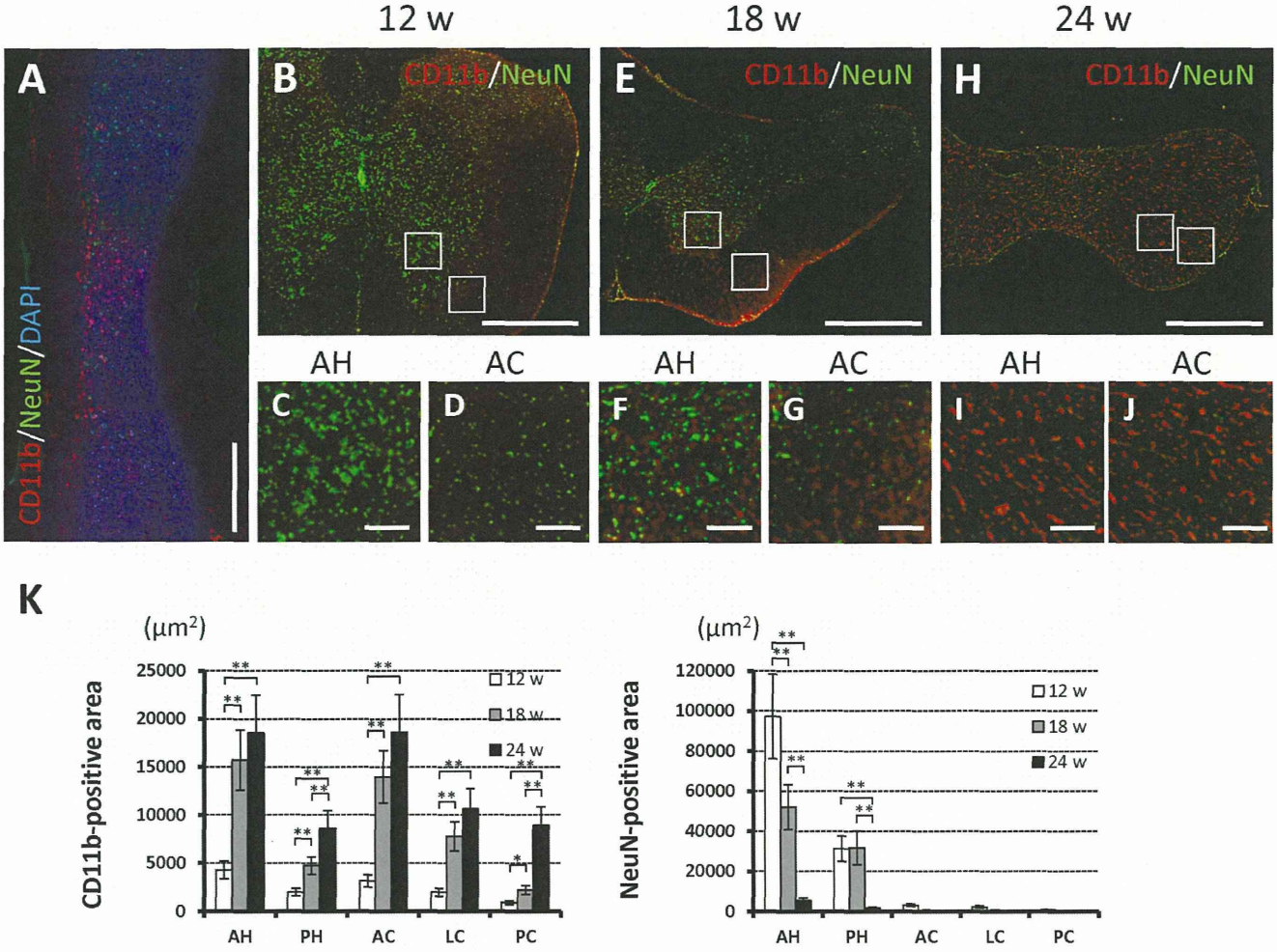

Figure 2. Increased prevalence of activated microglia/macrophages after spinal cord compression correlates to neuronal changes in *twy/twy* mice. Immunofluorescence staining for the expression of CD11b (red) and NeuN (green) in 12- (B–C), 18- (A, E–G) and 24-week-old (H–J) *twy/twy* mice. In sagittal sections of the spinal cords of 18-week-old *twy/twy* mice, CD11b-positive cells were distributed mainly in the sites of maximal compression site, compared with those sites that were rostral or caudal to the cord compression (A). The CD11b-positive area increased with the worsening of spinal cord compression, both in the gray and white matter, especially in the anterior horn (C, F, I) and anterior/lateral column (D, G, J). The NeuN-positive area of mainly the gray matter was especially lower in 24-week-old *twy/twy* mice (K). Scale bars = 500 μm (A, B, E, H); 50 μm (C, D, F, G, I, J). *$p<0.05$, **$p<0.01$ ($n=5$ for each time point). AH: anterior horn, PH: posterior horn, AC: anterior column, LC: lateral column, PC: posterior column. A–J microphotographs were taken using confocal laser scanning microscope.
doi:10.1371/journal.pone.0064528.g002

(Fig. 6C). Some neurotrophic factors and Mac-2 colocalized with arginase-1- or CD206-positive cells, whereas they did not with iNOS- or CD16/32-positive cells (Fig. 6). These results indicate that the M2 phenotype, but not the M1 phenotype, is a source of neurotrophic factors.

Helper T Cells, but not Neutrophils, Infiltrate the Chronically Compressed Spinal Cord

To evaluate the infiltration of neutrophils and helper T cells in the chronically compressed spinal cord, tissues were stained for MPO and CD4. No MPO-positive cells and very small amount of MPO activity were detected irrespective of the degree of spinal cord compression (Fig. S4), while the area of CD4-positive increased with advancement of spinal cord compression; especially in the gray matter of 18-week-old *twy/twy* mice (Figs. 7A–F). Few positive cells were seen in each age group of the control ICR mice and in 12-week-old *twy/twy* mice (Fig. S1C).

Increased Expression of Th2 Cytokines and Neurotrophic Factors in Chronically Compressed Spinal Cord

Western blotting was performed to evaluate the correlation between the severity of spinal cord compression and IFN-γ, TNF-α, IL-6, IL-4, IL-10, IL-13, BDNF, NGF, and Mac-2 protein levels (Fig. 8). IFN-γ (28 kDa band) was weakly expressed and its expression level did not change with age. The intensities of the bands of TNF-α (19 kDa band) and IL-6 (26 kDa band) increased with worsening of spinal cord compression (Fig. 8A). The intensities of the bands for IL-4 (18 kDa band), IL-10 (37 kDa band), and IL-13 (13 kDa band) reached peak levels in 18-week *twy/twy* mice, but somewhat decreased in 24-week *twy/twy* mice (Fig. 8B). The expression of these proteins in control ICR mice (with the same results seen in samples of different age groups; Fig. S2B) was the same as that seen in 12-week *twy/twy* mice. These results indicate increased Th1 cytokine expression reflects worsening of spinal cord compression, whereas increased Th2 cytokine expression

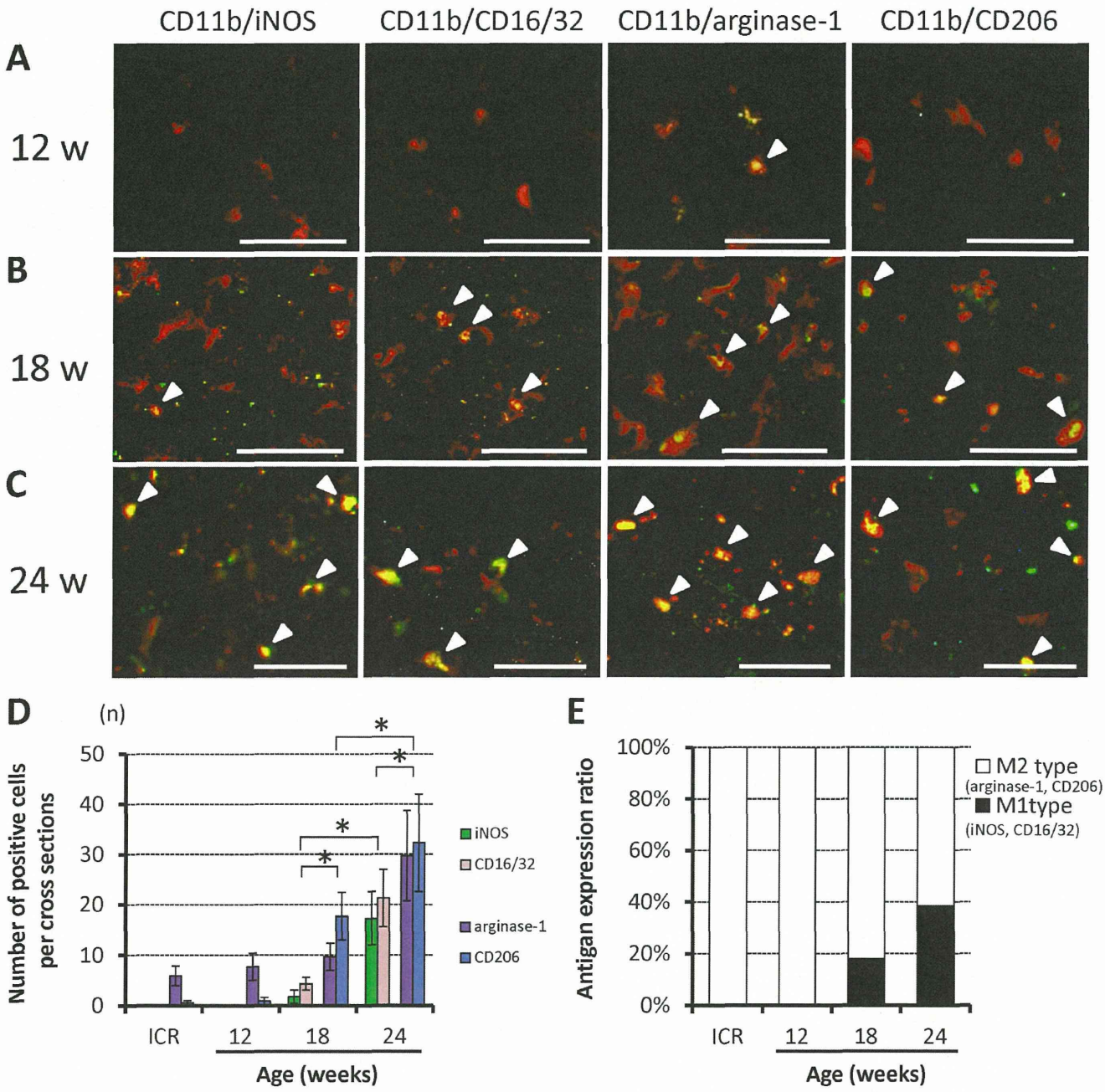

Figure 3. The prevalence of phenotypically activated microglia/macrophages in association with increased severity of spinal cord compression in *twy/twy* mice. Immunofluorescence staining for the expression of iNOS and CD16/32 (green) for classically activated microglia/macrophages (M1 phenotype) and arginase-1 and CD206 (green) for alternatively activated microglia/macrophages (M2 phenotype) co-localized with CD11b (red) in the anterior column of 12- (A), 18- (B) and 24-week-old (C) *twy/twy* mice. The numbers of CD11b-, CD11b/iNOS- and CD11b/CD16/32-positive cells (arrow heads) increased with the worsening of spinal cord compression. The CD11b/arginase-1- and CD11b/CD206-expressing cells (arrow heads) were the predominant population. The differences between iNOS, CD16/32 and arginase-1, CD206 were statistically significant in 18- and 24-week-old *twy/twy* mice. In control ICR mice, the expression of these factors was same as in 12-week-old *twy/twy* mice (D). The M1/M2 antigen expression ratio was higher in 24-week *twy/twy* mice compared with younger mice and control mice (E). Scale bars = 50 μm (A–C). Data are mean±SD. *$p<0.05$ (n = 5 for each time point). A–C microphotographs were taken using confocal laser scanning microscope.
doi:10.1371/journal.pone.0064528.g003

seems to reflect changes in the population of activated microglia. On the other hand, the intensities of the bands for BDNF and NGF, as well as Mac-2, increased significantly with advancement of spinal cord compression (Figs. 8C and D).

Discussion

We reported in the present study that chronic progressive compression of the cervical spinal cord due to a calcified lesion of the atlantoaxial membrane at C1–C2 in the *twy/twy* mouse caused neuronal loss, as indicated by NeuN-positive cells, an increase in CD11b-positive cells in both the grey matter and white matter,

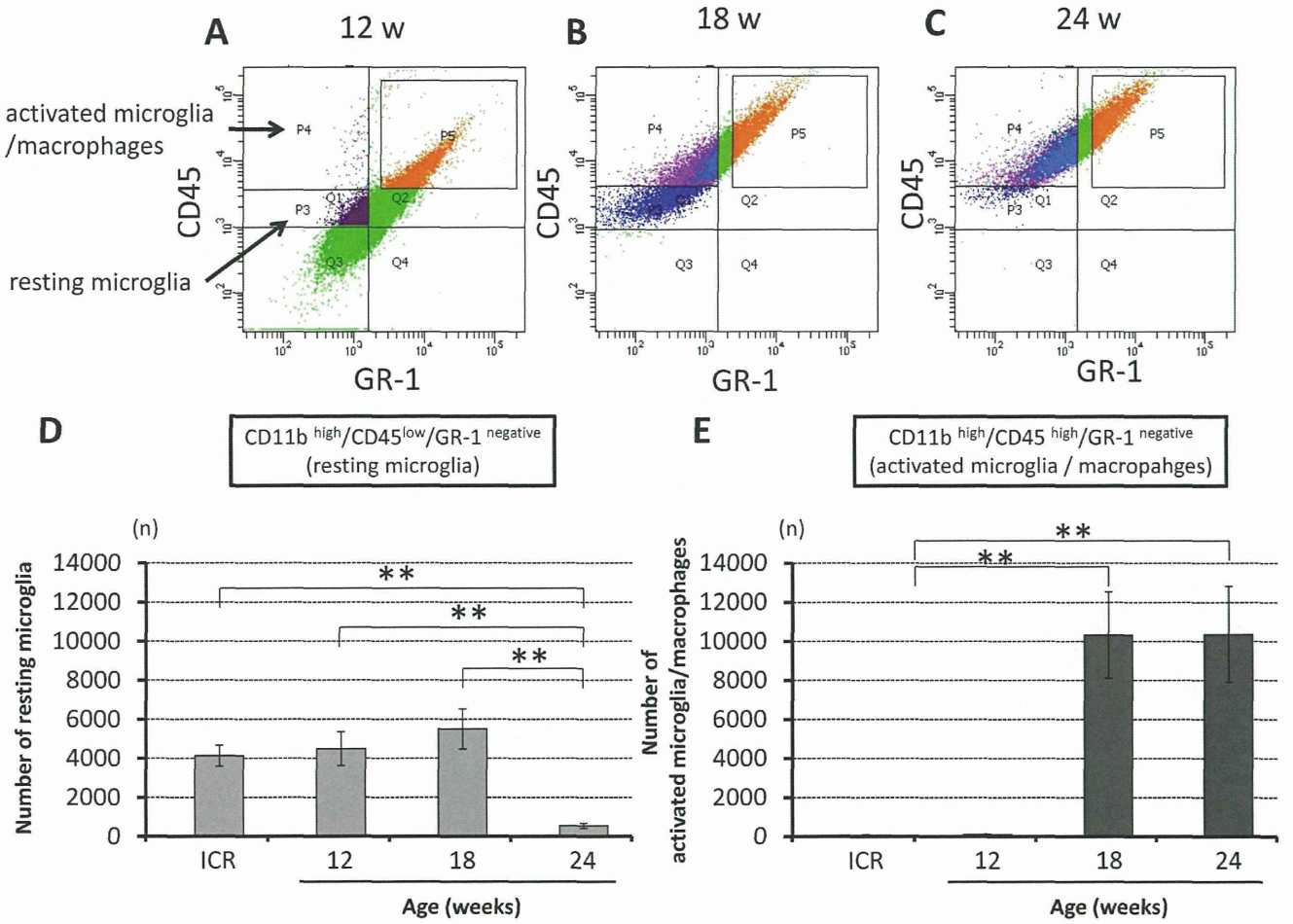

Figure 4. The resting microglia population decreased in association with increased severity of spinal cord compression in *twy/twy* mice. Semi-quantitative flow cytometric analysis of resting microglia and activated microglia/macrophages in the CD11b ^{positive} cells (10.4±0.7% of the spinal cord cells) according to the degree of spinal cord compression. Representative data for 12- (A), 18- (B) and 24-week-old (C) *twy/twy* mice. CD11b^{high} cells in the spinal cord were sub-fractioned into a CD45^{low}/GR-1^{negative} population, identifying them as resting microglia; or CD45^{high}/GR-1^{negative} population, which identified them as activated microglia/macrophages. The numbers of resting microglia (CD11b^{high}/CD45^{low}/GR-1^{negative} cells) were significantly lower in 24-week-old mice (D), while the numbers of activated microglia/macrophages (CD11b^{high}/CD45 ^{high}/GR-1^{negative} cells) were higher in 18- and 24-week-old *twy/twy* mice (E). The number of resting microglia and activated microglia/macrophages in control ICR mice was same as in 12-week-old *twy/twy* mice (D, E). Data are mean±SD. **p<0.01 (n = 3 for each time point).
doi:10.1371/journal.pone.0064528.g004

and infiltration of CD 4-positive cells in the grey matter as well as few MPO positive cells and the activity, with these changes seen at the site of the compression. The following are the main findings: 1) the number of CD11b positive microglia/macrophages increased with the severity of spinal cord compression; 2) there was a shift in the polarity of M1 and M2 cells present, with the prevalence of M1 cells increasing with the severity of spinal cord compression; 3) the number of resting microglia decreased in proportion with increases in activated microglia/macrophages; 4) arginase-1-positive cells, but not iNOS-positive cells, expressed neurotrophic factors (BDNF, NGF) and higher Mac-2 immunoreactivity; 5) an increase in Th1 cytokines increased with the severity of spinal cord compression, while an increase in Th2 cytokines was observed concurrently with changes in presence of the activated microglia population.

Several groups have characterized the pathological features of chronic spinal cord compression of patients with CSM and OPLL [5–7] or of the animal model of spinal cord compression seen in the *twy/twy* mouse [8,9,33–37]. Significant similarities in histopathological and pathophysiological changes have been described in chronic progressive spinal cord compression and traumatic SCI. These similarities include a decrease in the neuronal population with degeneration and demyelination followed by a cascade of "secondary" injury [2]. Activated microglia, derived from resting microglia, and recruited macrophages from the peripheral circulation are among the main effector cells of the inflammatory response that follows SCI, and are associated with the production of proinflammatory cytokines and related immune effector molecules that can induce both necrotic and programmed cell death, which correlate with neurological deficit [10,11,16]. Activation of microglia after SCI is evident on day one, and the number of activated microglia has been shown to increase during the first 7 days and then plateau, 2–4 weeks after injury; with small differences related to the animal strain being used as a model [13]. The present results demonstrated a decrease in the NeuN-positive area in the anterior horn opposite the posterior compression and posterior horn and an increase in the CD11b-positive area, especially in the anterior horn and anterior column; these changes were in proportion with the degree of spinal cord compression. In our previous studies, we observed a significant reduction in the

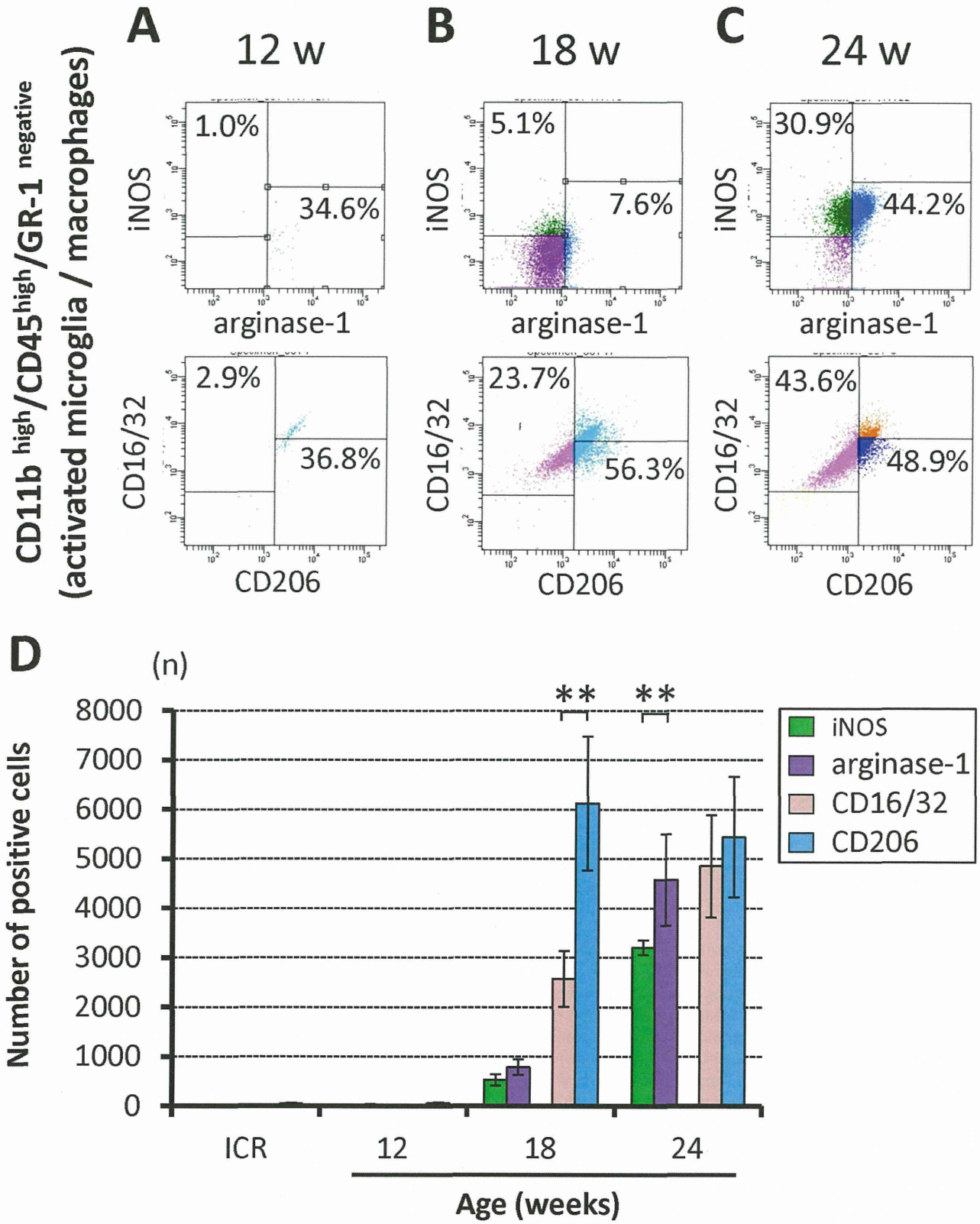

Figure 5. Expression of the M1 phenotype in activated microglia/macrophages correlated to increased severity of spinal cord compression in *twy/twy* mice. Semi-quantitative flow cytometric analysis of iNOS, CD16/32, arginase-1, and CD206 in activated microglia/macrophages. Representative data for 12- (A), 18- (B), and 24- (C) week-old *twy/twy* mice. The number of iNOS ^{positive} and CD16/32 ^{positive} activated microglia/macrophages increased with the worsening of spinal cord compression. Arginase-1 ^{positive} and CD206 ^{positive} cell populations were the predominant in cells present 18- and 24-week-old *twy/twy* mice (D). Data are mean±SD. **p<0.01 (n = 3 for each time point).
doi:10.1371/journal.pone.0064528.g005